DEPARTMENT OF INFORMATION ENGINEERING

Master degree in ICT for Internet and multimedia

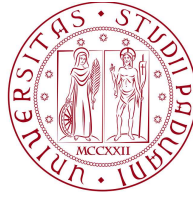## Localization of Metallic Lost Tools by Using UHF RFID Systems

Supervisor : Professor Leonardo Badia

Graduate student: Naoures Atidel Hamrouni

Co-Supervisor : Professor Baccar Sahbi
Professor Khalifeh Rania

ACADEMIC YEAR .2023 - .2024
Graduation date 10/15/2024

UNIVERSITY OF PADOVA

DEPARTMENT OF INFORMATION ENGINEERING - DEI

Master degree in ICT for Internet and multimedia

Localization of Metallic Lost Tools by Using UHF RFID Systems

Supervisor
Professor Leonardo Badia

Co-supervisor
Professor Baccar Sahbi
Professor Khalifeh Rania

Master Candidate
Hamrouni Nawres Atidel

Academic Year
2023–2024

ii

To my family, thank you for all your support, and advice. To my sister, who has always been supportive in every step of my life, I want to express my deepest gratitude for her continuous support and unconditional love. I wouldn't be where I am today without her by my side.

To my friends, Moni, Rania, Hanen, and Firas, you have been like a second family to me at every step. I dedicate this work to you, and I am truly grateful to have you by my side.

To my uncle's soul, you were my greatest supporter—may you rest in peace.

Abstract

The frequent loss of tools and parts, particularly metallic ones, presents significant economic and operational challenges in industrial settings, such as automotive manufacturing. This thesis explores the development of a robust system for locating lost metallic objects using RFID technology. Building on prior work, this study aims to validate the performance of a new RFID-based localization system and develop an efficient localization algorithm that addresses limitations identified in the existing literature. The research involves simulating proposed solutions in simple scenarios, followed by the implementation and testing of the algorithm in real-world conditions. Experimental results will determine if this system outperforms commercial alternatives in terms of signal strength and reliability. The developed localization algorithm is expected to exhibit high accuracy and rapid response times, significantly improving the efficiency of finding lost metallic objects. This integrated system holds potential for substantial improvements in industrial operations, reducing downtime and associated costs.

Contents

Listing of figures

Listing of tables

Listing of acronyms

6-DoF Degrees of Freedom

BFS Breadth-First Search

FSPL Free Space Path Loss

HF High Frequency

LF Low Frequency

LoS line-of-sight

NLoS non-line-of-sight

RFID Radio Frequency Identification

RSSI the Received Signal Strength Indicator

SNR Signal to noise ratio

UHF Ultra High Frequency

1
Introduction

The first chapter will briefly introduce the hosting institution where this thesis was conducted, followed by an overview of the subject's problem. Additionally, this chapter will outline the objectives and scope of the subject to facilitate understanding of the proposed work's topic.

1.1 Hosting Institution

This project was proposed and carried out in collaboration with the Institute for Research in Embedded Electronic Systems laboratory IRSEEM in Esigelec and Segula technologies.

1.1.1 The Institute for Research in Embedded Electronic Systems - IRSEEM

The Institute for Research in Embedded Electronic Systems - IRSEEM - is a Research Unit under the joint supervision of the ESIGELEC engineering school and the University of Rouen Normandy. It's located on the Rouen Normandy Science and Engineering Campus at the Madrillet Technology Park in Saint-Etienne du Rouvray, Rouen metropolitan area. IRSEEM's researchers combine their skills in electronics, automation, and computing to conduct scientific research that creates new knowledge and develops innovative technologies in response to the needs of industry and society. IRSEEM's research and innovation activities focus on the themes of energy transition, the industry of the future, intelligent mobility, and digital health, with applications in the automotive, energy, industrial, aerospace, biomedical, logistics, and telecommunications sectors.

1.1.2 SEGULA Technologies

SEGULA Technologies is a global engineering group serving the competitiveness of all major industrial sectors: automotive, aerospace, energy, rail, naval, life sciences, and telecoms. With a presence in more

than 30 countries and 140 locations worldwide, the Group is committed to building close relationships with its customers thanks to the skills of its 12,000 employees. As a leading engineering company that places innovation at the heart of its strategy, SEGULA Technologies carries out large-scale projects, from research through to industrialization and production.

1.2   Background and Context

In industrial settings, the loss of metallic tools and components is a frequent and costly issue. These losses can cause significant operational delays, increase downtime, and lead to heightened costs due to replacements. Also, metallic environments pose specific challenges for traditional localization systems, such as interference and signal reflection, which can make retrieving lost items even more challenging. The necessity for a reliable, efficient solution to locate metallic tools and parts within these environments is necessary. Addressing these challenges is at the core of this thesis, which aims to analyze a new approach using UHF RFID technology to enhance the accuracy and efficiency of locating lost metallic objects.

1.3   Objectives and Scope

The primary aim of this project is to validate and develop a new localization algorithm particularly designed for tracking metallic objects using UHF RFID technology. The main idea involves creating a robust and efficient algorithm tested with simulation to determine the location of lost tools in industrial settings accurately. The study focuses on metallic objects, which pose unusual challenges due to their reflective and conductive properties that can interfere with RFID signals. The research aims to address and overcome the limitations encountered in existing solutions, ensuring reliable and precise localization of metallic tools.

1.4   Thesis Structure

The thesis is organized as follows: Chapter 2 presents a literature review to provide an understanding of the main concepts and an overview of RFID technology. Chapter 3 details the methodology and results of our approaches. Finally, concluding remarks are provided in Chapter 4.

2

Literature Review

Radio Frequency Identification technology, which uses electromagnetic fields to identify and localize tags attached to different objects, has appeared as a promising solution to effectively localize lost tools in industrial settings. Despite its potential, the performance of Radio Frequency Identification (RFID) systems can be significantly hindered by metallic environments, which are prevalent in industries. This chapter provides a comprehensive review of the existing literature on RFID technology, it will begin with an overview of the fundamentals of RFIDtechnology, including its components, functionality, and various industrial applications, followed by the specific challenges posed by metallic environments. Next, the chapter discusses the state of the art in object localization, presenting an in-depth analysis of various localization methods in both general and metallic-specific contexts.

2.1 Overview of RFID Technology

The communication in the RFID system is established between the reader and the tag, and the information captured by the reader is generally distributed to a remote database. Also, the ID for an object: Electronic Product Code (EPC), allows us to identify the object in the database, this is specially used in chain management in warehouses. The concept of passive RFID communication is based on the retro-modulation or so-called backscatter principle [1]. An emitter radiates an electromagnetic wave with a given frequency and constant amplitude. This wave is both the energy source for the target or the tag and the retro-modulated wave support to send the tagID. In the other part, the receiver or the reader in reception mode demodulates the information message and then sends it to the database [2].

2.1.1 Basics of RFID: Components

Every RFID system is composed of three main elements: the tag transponder that embeds specific information about the item on which it is attached, and an antenna connected to a reader or interrogator that processes the information from the tag. After all the captured information is sent to a computer for further processing. All this interchange defines the base of the identification and tracking of objects using RFID technology. Figure 2.1 displays the basic features of the system. In this section, we will discuss the RFID components and specifications.
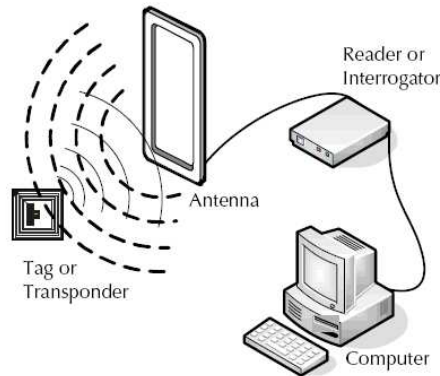
Figure 2.1: RFID system components.

RFID tags

RFID tags are the transponder units in the radio frequency identification system. It consists of an integrated chip to store a unique serial number and antenna.[3] The antenna is used to transmit the information from the integrated chip to the RFID reader. The tag's type of memory can be read-write, read-only, or write-once and read-many. Besides, RFID tags exist in three different versions: passive tags, active tags, and semi-passive / semi-active tags. [3]

   - **Passive tags**: Present the simplest version of RFID tags, without any power source, such as a battery, and it cannot initiate any communication with the reader. Passive tag derives its power from the energy waves transmitted by the reader and responds to the reader's radio frequency emissions, so the passive tag relies entirely on the reader's power source. Moreover, this tag should store a unique identifier for the item tagged and can be read from a range of about 0.1 to 0.5 meters. The cost of passive tags, which is generally low, varies based on the radio frequency used, and the amount of memory. [4]

- **Active tags:** Unlike passive tags, active tags contain a power source and a transmitter, in addition to the antenna and chip, and it send a continuous signal detected by the reader. These tags typically have read/write capabilities; tag data can be rewritten and/or modified. Besides, active tags can initiate communication and communicate over longer distances of up to 230 meters in ideal conditions. These tags contain more hardware than passive RFID tags, so they are more expensive and can reach 100 euros and more per tag so they are reserved for costly items that are read over greater distances.[1]

- **Semi-passive tags:** Semi-passive tags do not initiate communication with the reader but contain batteries

that allow the tag to perform other functions: monitoring the environment and powering the tag's internal electronics. To help conserve the battery lifetime, these tags remain dormant until they receive a signal from the reader. Furthermore, semi-passive tags can be connected to sensors to store information for container security devices.[5]

The following table 2.1 provides a detailed comparison of the key features of passive, active, and semi-passive RFID tags. This comparison covers aspects such as power source, communication range, cost, etc. Besides, figure 2.2 represents the physical differences between active and passive RFID tags, highlighting the existence of an internal battery in active tags which is absent in passive tags.

Feature	Passive Tags	Active Tags	Semi-Passive Tags
Power Source	No internal power source (powered by reader signal)	Internal battery	Internal battery for powering the chip, but uses reader signal for communication
Communication Range	Short range	Long range (up to 100 meters or more)	Medium range (up to 30 meters)
Cost	Cheap	Medium	Expensive
Battery Life	No battery (unlimited)	Limited by battery life (typically 3 to 5 years)	Limited by battery life (typically 3 to 5 years)
Size	Small and lightweight	Larger due to battery	Medium size
Typical Uses	Inventory management, asset tracking	Real-time location tracking, long-range applications	Environmental monitoring, condition tracking
Signal Strength	Weaker signal, relies on reader proximity	Strong signal, capable of longer distances	Strong signal, capable of moderate distances
Type of memory	Mostly Read-Only	read-Write	Read-Write
Life of tag	Up to 20 years	2 to 7 years	5 to 10 years
Environmental Impact	Susceptible to interference from metal and liquids	Less susceptible to environmental interference	Less susceptible to environmental interference

Table 2.1: Comparison of Passive, Active, and Semi-Passive RFID Tags [6]

RFID Reader

RFID Reader is a scanning device that reliably reads the tags and communicates the results to the middleware (computer or microcontroller). The reader has a proper antenna and uses it to communicate with the tag by broadcasting radio waves, as a result, all the tags within the range will respond.[3] Readers can process multiple items at once, allowing for increased read-processing times. They can be either mobile or stationary, and they are differentiated by their storage capacity, processing capability, and the frequency they can read.

Here we define the Components and Functionality of the RFID reader :
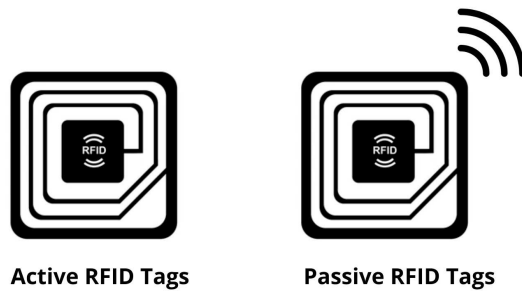
Figure 2.2: Active and Passive RFID tags

- **Antenna:** This is an important component of the RFID reader. It emits radio waves to interact with RFID tags and receives the signals that the tags send back. Depending on the reader design, the antenna can be integrated into the reader or be an external unit that can be positioned as needed.

- **Tag Communication:** readers use specific radio frequencies to communicate with tags. These frequencies can vary: Low Frequency (LF) , High Frequency (HF) and Ultra High Frequency (UHF).

- **Broadcasting and Receiving:** When the reader broadcasts radio waves, all RFID tags within the effective range respond by transmitting their unique identifier. This response allows the reader to process multiple tags at once, significantly increasing the read processing times.

The next table 2.2 provides an overview of the different frequency ranges used in RFID technology and highlights their respective descriptions and typical read ranges.

RFID Middleware

RFID middleware The middleware is the devices that connect the RFID readers and the data they collect, it helps make sense of RFID tag reads, and applies filtering and logic to the captured data. Some of the RFID middleware functions:

- **Data Filtering:** Not all data captured by RFID readers is necessary. Middleware applies filtering rules to discard irrelevant data. [7]

- **Data Interpretation:** RFID middleware interprets raw tag reads, converting them into a format other applications can understand.[8]

- **Security:** Middleware ensures that RFID data is transmitted securely and that only authorized personnel have access to the transmitted information by using encryption authentification and verification [6] .

RFID Antenna

RFID antennas are external components, interfacing devices that convert between electrical signals and electromagnetic wave propagations in free space. The antenna can help in the amelioration of the read distance and directionality of the RFID reader. In some readers, we may have an integrated antenna making it more compact but may limit the reading distance[3]. External antennas may play a crucial role in improving the performance the RFID systems. These antennas are connected to the reader via cables and can pointed to the tag localization, as a result, this can optimize signal strength and coverage. In the following figure 2.3,

Frequency	Description	Range	Advantages	Common Applications
Low Frequency (LF)	125 kHz or 134 kHz.	Up to 10 cm	Good penetration through water and biological tissues. Less sensitive to interference from metals and liquids.	Animal tracking, Access control, Smart cards
High Frequency (HF)	13.56 MHz.	Up to 1 meter	Moderate data transfer rate. Relatively unaffected by metal and liquids.	Smart cards, Ticketing, Data transfer
Ultra-High Frequency (UHF)	300 MHz to 3 GHz (commonly 860-960 MHz).	Up to 10 meters or more	Long read range. High data transfer rate.	Inventory tracking, Supply chain management, Asset tracking
Microwave	operate at frequencies typically in the GHz range, such as 2.45 GHz.	Very long read range (10 meters to 100 meters)	Long read ranges High data transfer rate	Electronic toll collection and certain types of asset tracking. However, they are highly sensitive to interference from environmental factors.

Table 2.2: Comparison of RFID Frequency Bands and Their Applications

we have an example of external antenna designs introduced by known suppliers like Zebra Technologies or Sparkfundation.

Figure 2.3: RFID External Antenna.

2.1.2 RFID Operating Principles and Application

RFID Operating Principles

The RFID systems rely on the interaction between tags and readers to function. The communication process involves the following steps shown in the following figure 2.4:

Step 1 : Electromagnetic Signal: This is the activation step, while the RFID reader emits an electromagnetic signal, which is shown as blue arrows. This signal powers passive RFID tags or activates active ones in the sounded environments and enables them to communicate with the reader.

Step 2 : Backscatter Modulation: The RFID tag uses backscatter modulation to reflect the reader's signal with slight modifications. This process is depicted by the green arrows. The modifications in the reflected signal encode the data stored in the RFID tag. Data Transmission: The tag sends the encoded data back to the reader. This data transmission process is essential for the RFID system to identify and track the tagged object.
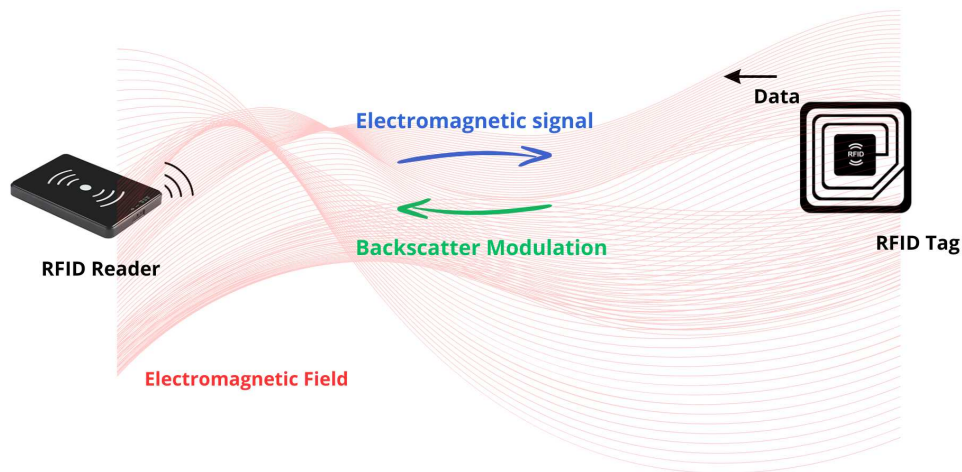
Figure 2.4: RFID Operating Principles

RFID Application in Warehouse Tracking

The radio Frequency Identification technology is widely used in warehouses and factories for tracking objects due to its efficiency and reliability. Our project focuses basically on enhancing this point and developing a solution using RFID for localization in warehouses. This technique can help in several points such as [9]:

- **The Improvement of Inventory Management**: It enables real-time tracking of tools and helps in reducing errors and discrepancies in stock levels.
- **Increased Efficiency**: Automating the process of inventory management helps minimize manual labor and speeds up some important operations.

- **Enhanced Accuracy**: This system can provide more accurate data on the location and movement of items compared to traditional barcode systems.
- **Security**: Enhanced tracking capability helps prevent theft and loss of goods.

Moreover, with the growth of this technology, it become more used in different applications and we can see that it was implemented and used in sever studies [3] [10]. There are some examples of application and implementation :

IoT and RFID in warehouse management [11]: One of the interesting applications is the development of a smart warehouse management system leveraging Internet of Things (IoT) technologies. The system uses Arduino and LORA for remote transmission and RFID tags for tracking warehouse goods. It integrates various sensors, including temperature, humidity, gas, and infrared sensors, to monitor warehouse conditions. A client interface was developed to allow users to monitor the warehouse status and manage inventory effectively. This smart system enhances efficiency, security, and real-time monitoring in warehouse management.

Finding objects in Household using UHF RFID Tags robot[12] : This solution developed a method for robots to find and navigate UHF RFID-tagged objects in household settings by optimizing RF signal strength. It combines global and local search strategies to maximize Received Signal Strength Indicator. IT demonstrates a high accuracy in locating tagged items without extensive data training. This approach enhances robotic efficiency in unstructured environments like homes. One of the important limitations in this study is that objects with a high metal content remained undetected, such as TV remote controls and keys (this limitation will be discussed in the next part)

2.1.3   RFID metrics

RFID metrics are essential parameters in evaluating the performance and effectiveness of RFID systems. These metrics are used to assess various aspects of RFID technology, particularly in object localization applications. To understand the effectiveness of RFID systems we need to comprehend the common RFID metrics used [13] :

- Received Signal Strength Indicator (RSSI) :

- The the Received Signal Strength Indicator (RSSI) is a well-known metric for measuring the strength of the signal received by the RFID reader from the RFID tag. It is often used to estimate the distance between the reader and the tag, a stronger signals generally indicating closer proximity. Furthermore, in localization algorithms, RSSI is an essential metric for determining the direction in which the RFID reader should move to approach the tag. [14]
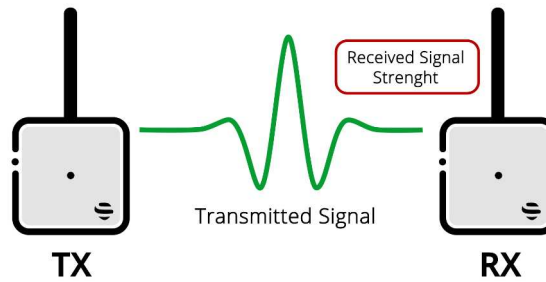
Figure 2.5: Received Signal Strength Indicator

- Signal-to-noise ratio (SNR):

- Signal to noise ratio (SNR) measures the ratio of the RFID signal's power to the background noise power. A higher SNR indicates a clearer, more distinguishable signal from the noise. In industrial environments, a high SNR is crucial for accurately detecting RFID tags. SNR impacts the accuracy of RSSI-based distance estimations in localization.[14]

- Latency :

- Latency is the delay between the RFID reader's request to read a tag and the receipt of the tag's data. In application, lower latency is preferable in real-time tracking and localization systems.

- Accuracy :

- Accuracy in RFID systems refers to the precision with which the system can determine the location of a tag or correctly identify a tag without errors, this can impact the ability to identify the exact position of an object within a defined area.

- Power Consumption :

- Power consumption is defined as the amount of energy required by the RFID reader and tags during operation.[13]

2.2 Environment Challenges

RFID technology is widely used in industry, but deploying it in application without consideration of the environment can potentially lead to a loss of money and time. In logistics and supply chain management, RFID tags are attached to goods stored on metal shelves, and on metallic tools, to ensure accurate inventory management during the transport and storage phases. Applying this technology on metallic surfaces can face various challenges that impact system performance and effectiveness. Metallic surfaces reflect electromagnetic waves, significantly impairing the performance of standard RFID tags.[15]

2.2.1 Effect of metallic objects on RFID performance.

Signal Reflection and Absorption

Metalic surfaces introduce the problem of the reflection and absorption of the signal generated by the RFID reader.

- Absorption: Metal absorbs RF signals, especially at higher frequencies such as those used in Ultra-high Frequency (UHF) , which lowers the strength of the signal received by the RFID tag or reader. Unfortunately, this phenomenon reduces the effective read range, limiting the distance over which tags can be detected and read [12].

- The Reflection: When an RF signal strikes a metallic surface, it is reflected in multiple directions. This reflection can cause the signal to travel along several different paths before reaching the RFID reader or tag. Studies have demonstrated using different objects shows a significant failure in localizing objects with metal components (for example keys, and metallic tools ..) [16]. This reflection leads to multipath interference and reduces the readability of RFID tags.

Detuning of Antennas

RFID antennas face important performance problems when they come into contact with materials like Metal or wood, which have similar dielectric properties. This interaction leads to detuning and a decrease in antenna gain. A study comparing dipole and slot antennas shows that the slot antenna's bandwidth is narrower and remains constant with detuning, whereas the dipole antenna's bandwidth increases with detuning. Both antennas experience similar levels of detuning and significant gain penalties as the material thickness increases [17]. In a warehouse with metal shelving and racks [18], RFID readers placed close to these metal structures may experience detuning. This can lead to reduced read ranges, making it harder to track inventory located on the shelves. Furthermore, tools with metallic packaging or components can detune RFID tags attached to them. This will reduce the effectiveness of the tracking phenomenon.

Shielding Effect

When a metal object is in proximity to an RFID wave antenna, the induced eddy currents within the metal by the time-harmonic magnetic field can oppose the magnetic flux generated by the antenna, which may significantly degrade its performance by shifting the resonant frequency and weakening the magnetic field inside the coil antenna. At this point, the metal objects can create a shielding effect. This phenomenon occurs when metal objects block RF signals entirely and prevent communication between RFID readers and tags [19] . Besides, this shielding effect reflects and absorbs the electromagnetic waves instead of allowing them to pass through (effect of shelves in the warehouse for example). This blocking is especially pronounced in the UHF range, where signals are more easily obstructed by conductive materials.

2.2.2 Effect of Liquid Environments on RFID performance.

Liquids, especially those with high water content, can interfere with RFID systems, especially high frequency [17]. Water absorbs UHF radio waves, which can reduce the read range and reliability of RFID

Limitations	Description
Size and Cost	Metal-mount tags are typically bulkier and more expensive than standard tags due to the additional materials and design complexity.
Range	The read range can still be shorter compared to non-metallic environments.

Table 2.3: Limitations of Metal-Mount RFID Tags

tags. Some studies showed that the presence of the liquid increases the loss resistance in the equivalent circuit of the antenna [20].

Signal Absorption

As the RF signal passes through the liquid, a significant portion of its energy is absorbed, which reduces the signal strength that reaches the RFID tag. This is especially pronounced at UHF frequencies, where the wavelength of the RF signals is close to the dimensions of the water molecules, leading to higher energy absorption [20]. In addition, the effectiveness of the read range is influenced, as a result, tags that could be read at a certain distance in a normal environment may only be detectable at a much closer range when it is surrounded by liquid. [17] .

Signal Scattering

Scattering refers to a signal falling on a rough surface and then traveling in multiple directions in a 3D space. Complete reflection happens when the surface is smooth like fluids. So we can say that liquids can scatter RF signals, causing unpredictable changes in signal direction and strength [20].

2.2.3 Existing solutions and their limitations

Metal-Mount RFID Tags

When it comes to RFID tags, mounting on or embedding in metal can be tricky, due to the metal interfering with the tag signal. RFID tag manufacturers have patented technology that allows RFID tags to work when attached to metal surfaces and even embedded within metal products. Metal-Mount RFID tags: These tags are specifically designed to function on or near metal surfaces. It includes a spacer or ferrite layer that separates the tag's antenna from the metal, reducing detuning and signal absorption.

Adaptive Antenna Designs in RFID Systems

Many studies work on designing an adaptive antenna that helps mitigate the effects of multipath interference and detuning. These particular studies mention the creation of an adaptive antenna using a cavity-backed slot antenna (C-BSA) coupled with an AKTAG loop antenna. [21], that have significantly enhanced RFID performance in metallic environments. This design utilizes the electromagnetic properties of cavities to mitigate detuning and signal degradation caused by metal surfaces. The optimized structure achieves improved

read ranges (up to 8 meters) and higher gains compared to traditional dipole antennas. This innovative approach provides a cost-effective solution for reliably tracking metallic objects, despite the specific design and placement requirements.

Limitations	Description
Added Complexity	The use of these materials adds complexity and cost to the RFID system.
Not Always Practical	Implementing RF-absorbing materials over large areas or in dynamic environments can be impractical.

Table 2.4: Limitations of RF-Absorbing Materials

RF-Absorbing Materials

Another solution is using specific materials that absorb RF energy. This can help in reducing reflections and multipath interference caused by any metal surfaces. In the market, many products have been introduced to fulfill this issue, for example, there is the RFID absorber, its a magnetic functional material with high magnetic permeability. It is usually made by uniformly filling some absorbents on polymer materials and making them through special processes. But these materials can be very expensive and not practical in large spaces [22]. This can help in reducing reflections and multipath interference caused by any metal surfaces. In the market, many products have been introduced to fulfill this issue, for example, there is the RFID absorber, its a magnetic functional material with high magnetic permeability. It is usually made by uniformly filling some absorbents on polymer materials and making them through special processes. But these materials can be very expensive and not practical in large spaces [19].

Temperature and Humidity

Extreme temperatures and high humidity can also affect RFID systems. Some RFID tags are specifically designed to withstand extreme temperatures, such as those used for tracking assets in cold chain logistics or high-temperature industrial processes. Similarly, RFID systems in high-humidity environments may require tags designed to withstand moisture.

2.3   State of the Art in Object Localization

As cited before, object localization refers to the process of determining the precise location of an object within a given space. Various technologies have been employed in industrial settings to locate the system accurately. RFID stands out due to its cost-effectiveness, energy efficiency, and suitability for indoor environments. This part will review existing localization algorithms and proposed solutions in the literature.

2.3.1 Solutions and Implementations

Article 1: A robotic system for the localization of passive UHF-RFID tagged objects on shelves

Our solution is based on a particular article, the first one is: **A robotic system for the localization of passive UHF-RFID tagged objects on shelves** [18].

The solution presented in the article uses a robotic system to locate RFID-tagged objects on shelves in a warehouse environment autonomously, while the authors describe a robotic system that uses an electromagnetic model to estimate the position of the tagged objects. The main idea is that an ultra-high frequency RFID reader is attached to the robot, As it moves in front of the shelves, the reader continuously emits radio frequency signals and listens for the backscattered signals from RFID tags on the shelves. Each tag modulates the backscattered signal by altering its impedance state, creating a signal that can be detected by the RFID reader. The reader records the phase of the backscattered signal at each position along the robot's path.

This article model is divided into 4 core steps :

1. Signal Phase Collection

2. Electromagnetic Model

3. Position Estimation

4. A Two-Step Process.

During its path, the robot collects the phase measurements $\phi_{\text{reader}}(s(t))$ at assigned time instants t_i corresponding to known positions $s_i = (x(t_i), y(t_i), z_R)$ for $i = 1, \ldots, N$ of its trajectory. The discrete pattern of measurements is denoted by $\{\phi_i\}$, where each element $\phi_i = \phi_{\text{reader}}(s_i)$ can be modeled as:

$$\phi_i = \text{mod}\left(-2K\sqrt{(x_i - x_T)^2 + y_i^2 + (z_R - z_T)^2} + \phi_{rM}(s_i) + \phi_d + \theta_n, \pi\right) \qquad (2.1)$$

This equation can be broken down into the following components:

- ϕ_i**:** The phase measurement at the i-th position along the robot's trajectory.

- **mod**$(\cdot, \pi)$: The modulus function that computes the phase modulo π. This function ensures that the phase is wrapped within a range of 0 to π, accounting for the inherent ambiguity in phase measurements.

- $-2K$**:** A scaling factor related to the wavelength of the RFID signal, where $K = \frac{2\pi}{\lambda}$ and λ is the wavelength.

- $\sqrt{(x_i - x_T)^2 + y_i^2 + (z_R - z_T)^2}$: The Euclidean distance between the RFID reader at position (x_i, y_i, z_R) and the tag at position $(x_T, 0, z_T)$. This is the primary term influencing the phase shift due to distance.

- $\phi_{rM}(s_i)$**:** A term representing the multipath effects or reflections at position s_i along the robot's trajectory. This term introduces additional phase shifts due to the environment's influence.

- ϕ_d: A constant phase offset that accounts for any phase shifts introduced by the RFID reader's hardware or other constant factors in the system.

- θ_n: The noise in the phase measurement. This term is typically modeled as a random variable with a mean of zero, contributing to the overall uncertainty in the phase measurement.

The objective is to estimate the coordinates (x_T, z_T) of a tag, knowing only the set of reader positions $\{x_i, y_i, z_R\}$. Neglecting for a moment the noise terms in Equation 2.1, it is clear that for a particular trajectory $y_i = y_R = $ constant (i.e., a trajectory parallel to the shelf), the minimum tag-reader distance is achieved when $x_i = x_T$. Thus, phase measurements present a local maximum at this position, which is also a center of symmetry for the phase pattern $\{(x_i, \phi_i)\}$.

Different values of $(z_R - z_T)$ do not change the position of this maximum but only shift its level, so that tags having the same x_T but different z_T are distinguishable by the level of the maximum of their phase pattern if the ϕ_d term were absent or known. Instead, ϕ_d and the periodicity of the modulus function make the knowledge of z_T ambiguous. On the other hand, if $|y_R|$ is sufficiently large with respect to $|z_R - z_T|$, a small change in z_T does not significantly modify the shape of the phase pattern. The estimate of x_T, therefore, is not ambiguous and is independent of both z_T and ϕ_d.

So, we choose the trajectory $y_i = y_R$ to collect a set $\{\phi_i\}$ of measurements to be used for estimating x_T. The effect of the noise terms ϕ_{rM} is a deformation of the shape of the phase pattern (i.e., it may lose its symmetry) because it is correlated over sets of nearby points, while θ_n changes randomly the value of each ϕ_i. The noise θ_n can be modeled as a Gaussian random variable with a null mean, while the variance can be determined a priori based on the characteristics of the hardware. The perturbation introduced by ϕ_{rM} is deterministic but strongly dependent on the geometrical and morphological details of the particular setup. Furthermore, it is dependent on the unknown position of the tag, so a deterministic model is not possible. However, if the noise is not excessively strong, the shape of the phase pattern is preserved since it is defined by x_T and z_T only.

The estimate of x_T can be performed by searching for the noiseless phase pattern that best fits the measured one among a number of realizations of noiseless phase patterns calculated over a given domain of x_T and z_T. Let $\Delta\phi_i$ denote the difference between the phase measurements ϕ_i and the noiseless realized ones $\phi_{p_i}(x_T, z_T)$:

$$\Delta\phi_i(x_T, z_T) = \phi_i - \phi_{p_i}(x_T, z_T) \qquad (2.2)$$

For each possible position (x_T, z_T) of the tag on the shelf (assuming $x_T \in (x_{T,\min}, x_{T,\max})$ and $z_T \in (z_{T,\min}, z_{T,\max})$, and considering a quantization step q_x and q_z for the x and, respectively, the z coordinates of the tag), the total phase discrepancy is given by the norm of the vector $\Delta\Phi(x_T, z_T) = (\Delta\phi_1, \dots, \Delta\phi_N)$. The coordinate x_T is estimated as:

$$\hat{x}_T = \arg\min_{x_T, z_T} \|\Delta\Phi(x_T, z_T)\| \qquad (2.3)$$

The uncertainty of the estimate $\hat{x}_T$ is related to the noise and can be evaluated a priori.

Once the estimate $\hat{x}_T$ is available, we exploit the other degree of freedom of Equation 2.1, i.e., the orthogonal movement $x_i = $ constant, to estimate the coordinate z_T. The robot performs a path along the trajectory $x_i = \bar{x}_R$ to collect a new set $\{\phi_j\}_\perp$ (for $j = 1, \ldots, M$) of measurements. Applying the best fit criterion on the (z_T, ϕ_d) plane, we estimate both $\hat{z}_T$ and $\hat{\phi}_d$ as:

$$(\hat{z}_T, \hat{\phi}_d) = \arg \min_{z_T, \phi_d} \|\Delta\Phi(z_T, \phi_d)\| \tag{2.4}$$

where $\Delta\Phi(z_T, \phi_d)$ is the discrepancy vector whose M elements are $\Delta\phi_j(z_T, \phi_d) = \phi_j - \phi_{h_j}(z_T, \phi_d)$ and $\phi_{h_j}(z_T, \phi_d)$ is given by:

$$\phi_{h_j}(z_T, \phi_d) = \mathrm{mod}\left(-2K\sqrt{(\bar{x}_R - \hat{x}_T)^2 + y_j^2 + (z_R - z_T)^2} + \phi_d, \pi\right) \tag{2.5}$$

The search over the (z_T, ϕ_d) plane is very sensitive to the variation of z_T but not to that of ϕ_d, so we can obtain an accurate estimate of z_T while ignoring ϕ_d, which is not the subject of estimation.

The following flowchart 2.6 illustrates the process of the robotic localization of UHF-RFID-tagged objects on shelves.[18]

The implementation involves a robot equipped with an RFID reader as shown in figure 2.7 and a carefully designed algorithm that operates in two main stages.

1. In the first stage, the robot localizes itself within the warehouse. This is done using a **Kalman filter-based algorithm** [23] (A Kalman filter-based algorithm is a recursive estimation method that optimally combines a measurement sensor with a predictive model to estimate the true state of a dynamic system.) The algorithm fuses odometry data with the phase information obtained from reference RFID tags placed along the shelves. These reference tags provide fixed points of known location, helping the robot accurately determine its position relative to the shelves.

2. In the second stage, once the robot's location is established, it begins locating the RFID-tagged objects on the shelves. The robot follows two specific paths one parallel to the shelves and one perpendicular. As it moves, the robot collects phase measurements from the RFID signals emitted by the tagged objects. These measurements are then matched to a pre-defined parametric electromagnetic model, allowing the system to accurately determine the location of the objects on the shelves.

The key innovation in this article lies in the configuration of the robot's movement paths, which are optimized to decouple the estimation of different tag coordinates. By combining an electromagnetic model into this process, the system simplifies the computational complexity and significantly improves the precision of the localization of the tagged object. So this model allows the robot to accurately interpret the phase data collected along these optimized paths, leading to precise estimations of the tag positions even in challenging environments.
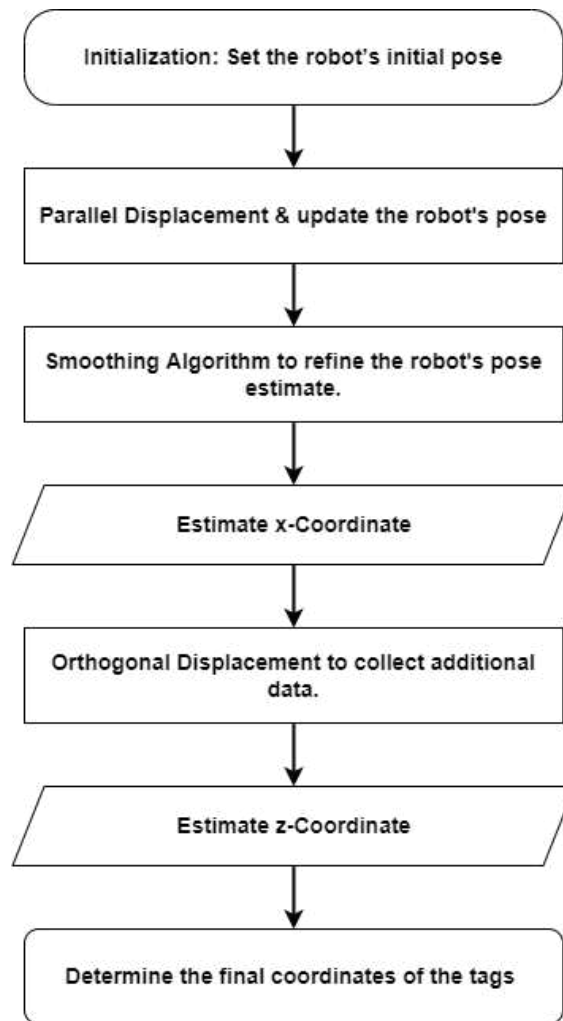
Figure 2.6: Flowchart illustrating the process of robotic localization of UHF-RFID tagged objects on shelves

Article 2 : Finding and Navigating to Household Objects with UHF RFID Tags by Optimizing RF Signal Strength

In our second reference [12], the authors present a solution that involves formulating the task as an optimization problem, where the robot must find a pose of a directional antenna that maximizes the Received Signal Strength Indicator RSSI from the target RFID tag. The implementation consists of these key behaviors: A Sparse global sampling is employed in this solution to first identify the vicinity of the tagged object, enabling the robot to check down the search area by sampling RSSI values all over the loo. Once a general location is identified, bearing estimation refines this by determining the precise direction of the tag, leveraging the directional capabilities of the robot's antenna.

This method allows the robot to orient itself accurately toward the object. Following this, the RFID serving guides the robot as it approaches the tag, continuously adjusting its path to maximize the RSSI signal.

17
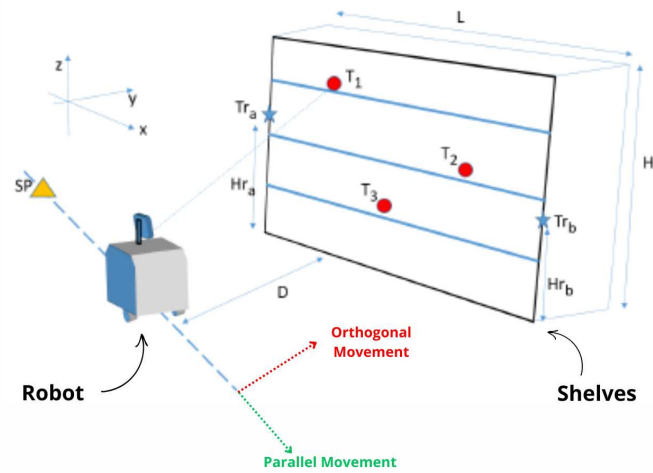
Figure 2.7: 3D view of the phase collection process.

These behaviors collectively exploit the directional nature of the antenna and the variability in RSSI, allowing the robot to navigate efficiently through the room environments. This technique eliminates the need for extensive training data or complex sensor models, making the system robust and adaptable to different settings. The system was tested in a realistic home environment using a PR2 robot that uses two actuated, shoulder-mounted UHF RFID antennas are shown in the figure 2.8. It successfully demonstrates the ability to locate various tagged household objects with high accuracy and reliability.
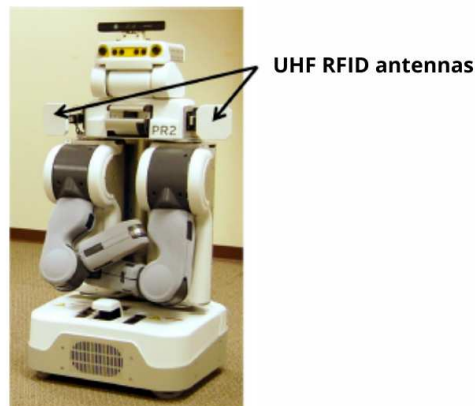
Figure 2.8: PR2 robot with mounted UHF RFID antennas to search for tagged objects

The author presents the optimization problem in [12] as a mathematical function presented as:

$$P^* = \arg\max_P E(\text{RSSI} \,|\, P = P)$$

where:

- P^* : the optimal pose (position and orientation) of the PR2 robot.

- P : a Degrees of Freedom (6-DoF) pose, which includes both the 3D Cartesian position and the orientation angles of the PR2 antenna.

- $E(\text{RSSI} \,|\, P = P)$ is the expected value of the RSSI given the pose P.

The core key Points of this optimization are :

- **Sampling of RSSI:** The robot physically moves to different poses in the room while recording the RSSI from different objects in the environment. After, all the RSSI values are treated as samples.

- **Global Search:** The PR2 robot conducts a global search over a constrained plane, it samples different postures in a specific spot in the environment. this search enables the robot to get close to the target by identifying areas where the RSSI is relatively strong.

- **Local Search :** Once the robot is in the area of the tagged object (this is based on the global search), it refines its position using a local search. Moreover, it adjusts its orientation to maximize the RSSI, effectively homing in on the tag.

- **Servoing Behavior:** In some cases, the robot uses the two antennas shown in the figure 2.9, pointed in different directions to estimate the gradient of RSSI. The difference in RSSI between the two antennas gives an idea about the direction that the robot should take to increase RSSI. The PR2 drives along and adjusts its heading based on the difference in signal strength detected by the two antennas and continuously updates its pose to maximize the RSSI.

The following flowchart 2.9 illustrates the process of robotic localization and navigation to UHF-RFID-tagged objects using sparse sampling.
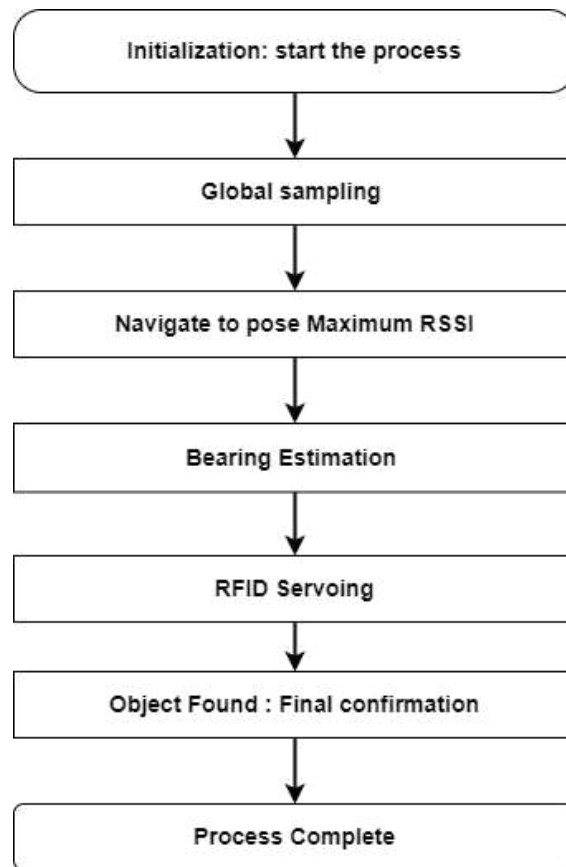
Figure 2.9: Flowchart illustrating RFID Tagging and Navigation Process using a moving robot

2.3.2 Limitations

- **Multipath Interference and Signal Distortion** :

Both solutions [18] [12] are significantly affected by multipath interference, [24] particularly in environments with metallic objects. In such environments, RF signals can reflect off surfaces, causing phase distortion and signal degradation, which leads to inaccuracies in the localization of RFID tags. This issue is prevalent in both the warehouse scenario described in the first article and the household environment in the second article.

- **Tag Detection Failure**:

- The article [12] highlights specific challenges in detecting tags on or near metallic objects, such as keys or a TV remote, even when using tags designed for metal surfaces. In some cases, these objects were not detected at all, leading to failures in the localization process.

- **RSSI Variability**:

- Both articles discuss the inherent variability in RSSI due to noise, stochasticity introduced by communication protocols, and the complex interactions between the RF signal and the environment. This variability can complicate the optimization process and lead to less reliable localization outcomes.

These limitations highlight the ongoing challenges in developing robust RFID-based localization systems that can consistently perform well in diverse and complex environments. Our study will specifically focus on addressing these limitations, aiming to develop a more robust approach that mitigates the impact of environmental factors on RFID-based localization systems

2.4 Conclusion

This chapter provided a comprehensive overview of RFID technology, its basics, and its important components. The review highlighted the significant challenges that metallic environments pose to RFID systems, such as signal reflection and absorption, which can severely impact the accuracy and reliability of object localization. Furthermore, this chapter introduces solutions explored in the literature, including developing specialized algorithms though each comes with its limitations. In summary, this chapter establishes a solid foundation for building our solution and the validation of a novel RFID localization system by identifying the critical shortcomings of current technologies. This sets the stage for the methodology and experimental work to be discussed in subsequent chapters.

3

Methodology

This chapter details the methodological framework employed to develop and validate the RFID-based localization system for metallic lost tools. The methodology is structured to address the limitations identified in existing solutions and to ensure the proposed algorithm's effectiveness in challenging metallic environments. The development process includes several key phases: the design and adaptation of the localization algorithm, simulation of the proposed solution in controlled scenarios, and experimental validation in real-world conditions. Each phase is meticulously planned to refine the algorithm, enhance its robustness against environmental challenges, and assess its performance against commercial alternatives. This study aims to produce a reliable and efficient tool localization system for industrial applications by systematically testing and optimizing the algorithm.

Developing the localization algorithm involves several steps, including adapting existing methods to account for the unique challenges posed by metallic environments. This section details the algorithm's design, the modifications to enhance its performance, and the theoretical underpinnings of these changes. For this work, 2 algorithms were defined and simulated to see the effectiveness of it.

3.1 Methodology and Development of Algorithm A

3.1.1 Main Concept and Design Principles

The proposed idea revolves around localizing an object tagged with RFID in a controlled environment, like a room where we know the height and width. Starting with a simple case, we can define a 4x4 room where the door is the reference point (0, 0, 0). The coordinate system is based on the Cartesian reference system. (X, Y, Z) .

The tagged object, denoted as O, has known coordinates in the room defined by

$$O = (X_O, Y_O, Z_O)$$

where the height of the object (z-coordinate) is already determined (in the next steps we suppose the object is on the floor to facilitate the situation of localization so $z_O = 0$).

The main goal is to locate the tagged object's X_O and Y_O coordinates within the 2D plane. The user, equipped with a tablet containing an RFID reader, enters the room through the door and attempts to detect the RFID tag on the object to localize it. we suppose the user's coordinates are :

$$U = (X_U, Y_U, Z_U).$$
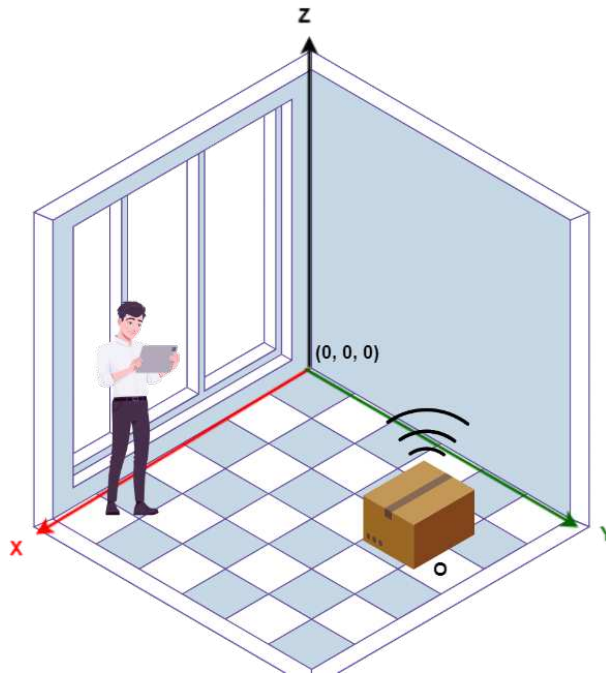
Figure 3.1: Visualization of RFID-Based Object Localization Algorithm A

To achieve this, the proposed algorithm employs a Breadth-First Search (BFS) approach to explore the room efficiently. The BFS method starts at the door (0, 0). It systematically examines adjacent grid points to detect the object's RFID signal, using theRSSI as the guiding metric. The algorithm measures RSSI at adjacent points (e.g., (1, 0) and (0, 1)) and uses this information to decide the next point to explore. The exploration process continues, marking each grid point as explored until the object is located.

This approach thoroughly searches the entire room, minimizing the chances of missing the object. The BFS strategy, combined with the grid-based movement and signal measurement, provides a structured and reliable method for locating the object within the room. This approach not only leverages the directional nature of RSSI but also ensures that the search process is both systematic and exhaustive, covering all possible locations in the grid-based environment.

3.1.2 Operational Workflow and Implementation

As we mentioned, Algorithm A is designed to localize tagged objects within a defined grid environment using a Breadth-First Search (BFS) strategy, while this method leverages the RSSI to systematically explore the grid and accurately determine the object's location. The following flowchart 3.2 gives a general idea of the algorithm. The flowchart 3.2 illustrates the decision-making process for localizing an object within a grid-based environment using RSSI measurements. The algorithm begins at the starting node, positioned at coordinates (0,0) which is the door of the room.

Figure 3.2: Algorithm A: Step-by-Step Execution Flow

• **Sequence Diagram**:

The sequence diagram in figure 3.3 illustrates the operational workflow of our algorithm. As we mentioned the algorithm utilizes a Breadth-First Search strategy combined with the RSSI measurements to determine the object's position on a grid.
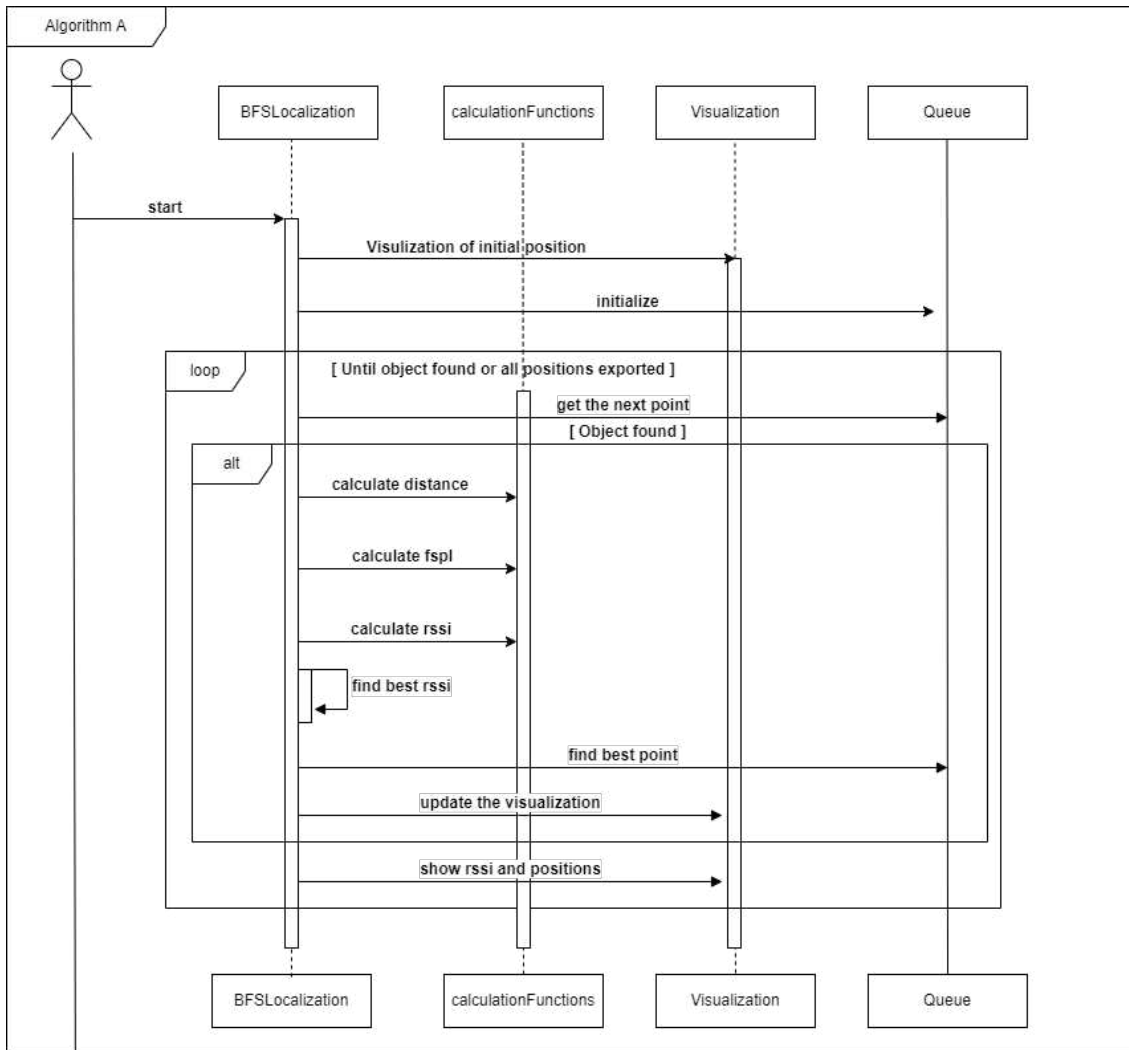
Figure 3.3: Sequence diagram of the algorithm A

    1. Starting by Looping Through the Grid Points: The algorithm starts by iterating through the grid using a BFS approach. The user begins at the starting point and systematically explores adjacent grid points.

2. RSSI Calculation: At each grid point, the algorithm measures the RSSI values from the adjacent points to estimate signal strength.

3. Alternative Paths: According to the RSSI values [16] , new direction with the strongest signal can be chosen for additional exploration.

4. Visualization: A visualization is a must in our simulation to see the algorithm's functionality.

5. RSSI and Position: Throughout the process, the RSSI values and grid positions are continuously monitored and displayed, guiding the user toward the object. The loop continues until the object is located, signified by the strongest RSSI reading at the object's position.

The sequence diagram provides a straightforward step-by-step representation of how the proposed solution

systematically searches for and localizes the object within the environment.

- **Visual Observation**:

Before moving, the user visually scans the immediate surroundings to get an initial idea of the object's potential location based on visual cues or prior knowledge. There is a possibility that the object is around the user. The following image illustrates the first observation step 3.4 .
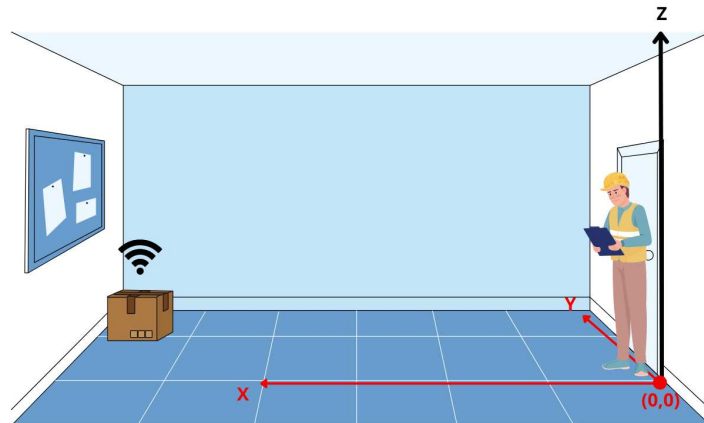
Figure 3.4: Algorithm A:Visual Observation

- **Grid-based Movement and Signal Measurement**

In the proposed scenario, the environment is represented as a grid with labeled coordinates. Each cell in the grid corresponds to a specific (X, Y) position. The user starts at the origin point (0.0, 0.0). The object is placed at a target location, and the user's goal is to navigate through the grid, step by step, using signal strength RSSI metrics to locate the object.

1. **Initial Position (0.0, 0.0)**: The user begins from the door, where the position is labeled as (0.0, 0.0). From this starting point, the algorithm evaluates the signal strength (RSSI) at adjacent positions to decide where to move next.

2. **Adjacent Point Exploration**: At each step, the user measures the RSSI at adjacent points. For example, from the starting point (0.0, 0.0), the adjacent points (0.1, 0.0) and (0.0, 1.0) are explored. The algorithm then compares the signal strength from these two points.

3. **Selecting the Best Direction:** Based on the RSSI readings, the user moves to the adjacent point with the stronger signal. In the second step, the user may move from (0.0, 0.0) to (0.1, 0.0) if the signal is stronger in that direction, or to (0.0, 1.0) if that direction offers a stronger signal.

4. **Grid Navigation:** The user continues navigating through the grid, repeating the process of evaluating RSSI at adjacent points and selecting the next move based on the highest RSSI reading. The path may vary based on the object's location and signal strength distribution.

5. **Final Position:** The process continues until the user reaches the grid cell where the object is located. Once the object is found (when the RSSI indicates the strongest signal), the algorithm terminates the search.

So in summary this step involves measuring the RSSI at two adjacent points each time to determine which direction offers a stronger signal as mentioned in figure 3.5 and based on the comparison, the algorithm selects the direction with the stronger RSSI for further exploration.
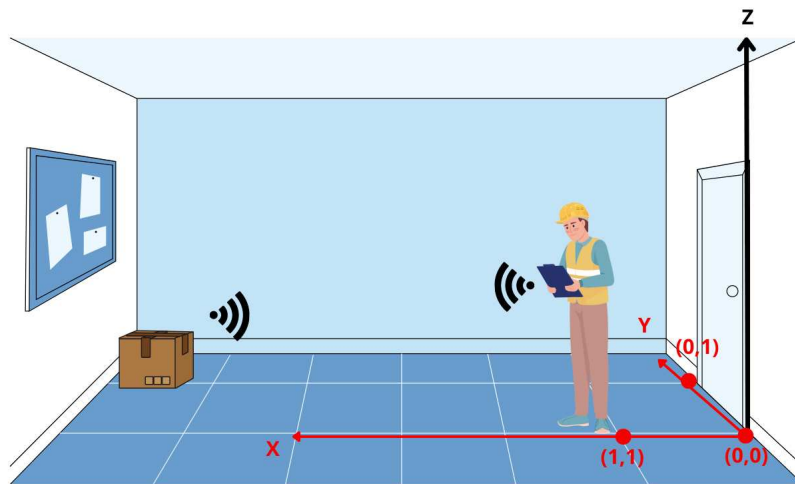
Figure 3.5: Algorithm A: Grid-based Movement and Signal Measurement

3.1.3 Simulation Setup for Algorithm A

As the solution is proposed for a company operating in an industrial environment, the robustness and accuracy of the suggested algorithm need to be thoroughly tested under various conditions similar to resembling real scenarios. Industrial settings often present challenges, especially interference from metallic surfaces, and signal reflections. To ensure that Algorithm A can reliably localize objects in such environments, it is essential to perform rigorous testing before deployment. A simulation setup for Algorithm A has been designed specifically to evaluate the effectiveness of the algorithm in localizing objects within a defined grid environment using RFID signal strength metrics. This simulation aims to reproduce key aspects of industrial environments.

- **Parameter Definition for Scenario Testing**

The first step was to define all the necessary parameters to simulate the scenario effectively. One of the key metrics to assess in this scenario is the RSSI at each step of the user's movement. The RSSI is a measure of the signal strength at the receiver and is calculated using the transmitted power and Free Space Path Loss (FSPL).

- **RSSI Calculation**: The RSSI is computed by subtracting the Free Space Path Loss (FSPL) from the transmitted power (`txPower`). The RSSI can mathematically be expressed as follows:

$$RSSI = txPower - FSPL \tag{3.1}$$

Where:

- `txPower`: The power of the transmitted signal, typically measured in dBm (decibels).

- `FSPL`: The Free Space Path Loss, representing the loss of signal strength as the signal propagates through free space, measured in decibels (dB).

The RSSI indicates how strong the received signal is after accounting for the signal loss due to distance and other factors. A higher RSSI value indicates a stronger signal at the RFID reader.

- **Free Space Path Loss Calculation:** To compute the RSSI, the Free Space Path Loss must be calculated. FSPL measures how much the signal strength decreases as it travels through free space. The FSPL is dependent on the distance between the transmitter and the receiver, as well as the frequency of the transmitted signal. The FSPL can be given by the following equation:

$$FSPL = 20 \log_{10}(d) + 20 \log_{10}(f) - 147.55 \tag{3.2}$$

Where:

- d: The distance between the transmitter and the receiver, measured in meters.

- f: The frequency of the transmitted signal, measured in MHz.

- 147.55: A constant used to account for the speed of light and conversion factors in the free space loss formula.

The FSPL value is essential in determining how much signal power is lost over the distance, and it directly impacts the RSSI calculation.

- **Distance Calculation:** The third step involves determining the distance between the user's current position and the next point that the user will move to. This is necessary to update the FSPL and RSSI values as the user moves within the environment. The distance between two points in a 2D plane can be calculated using the **Euclidean distance** formula, as follows:

$$d = \sqrt{(x_{\text{user}} - x_{\text{next}})^2 + (y_{\text{user}} - y_{\text{next}})^2} \tag{3.3}$$

Where:

- $x_{\text{user}}, y_{\text{user}}$: The coordinates of the user's current position.

- $x_{\text{next}}, y_{\text{next}}$: The coordinates of the next point the user will move to.

By recalculating the distance at each step of the user's movement, the FSPL can be updated, and consequently, the RSSI can be recalculated to reflect the signal strength at each new position.

3.1.4   Results of the Localization Algorithm A

The following figures illustrate the execution of the localization algorithm. The user starts from an initial position (red dot) in the grid and moves toward the object, located at a fixed point (green dot), using the Received Signal Strength Indicator metric to guide each move.

Initial State: The first figure 3.6 shows the user's initial state.

- The user starts at the origin position (0,0) presented by the red dot. The object is placed at position (5,6), marked with a green dot. No moves have been made yet, and the process is about to begin.
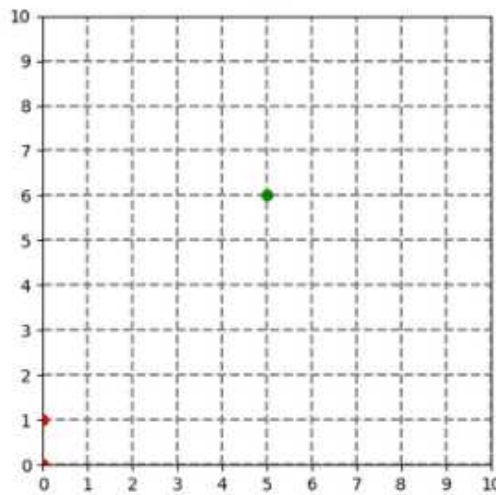
Figure 3.6: Initial State: Starting Position of User and Object

Intermediate Steps :

- The algorithm begins exploring neighboring points based on the calculated RSSI values.

30

- As the user moves, the path is traced in red, this helps to follow the best path to find the object as shown in figure 3.7. In this step, the user has moved a few steps closer to the object's location by examining the neighbors that's why it's similar to the BFS process.
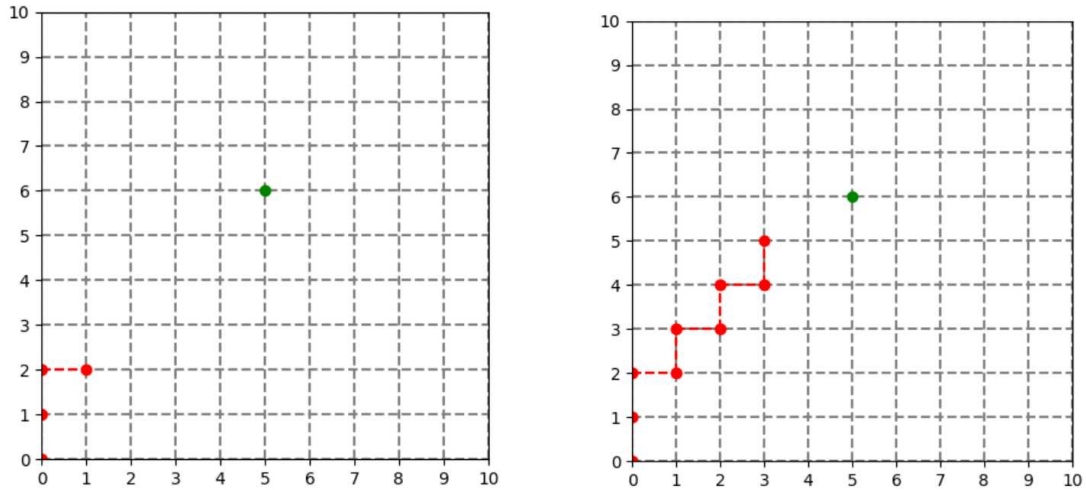
Figure 3.7: Intermediate Steps: User Exploring the Grid

Final Path :

- The user successfully reaches the object.
- The red line represents the complete path taken by the user to reach the object as seen in the following image 3.8. The movement is guided by RSSI values calculated at each step.

This figure 3.9 shows the Received Signal Strength Indicator vs. Grid Position as the user moves through the grid toward the object using a BFS-based localization algorithm.

Initially (area 1 in figure 3.9) The RSSI values are around -40 dBm in the initial grid positions (e.g., (0,1), (1,0)), indicating that the user is far from the object, and the signal is weak. after we can distinguish a gradual signal amprovement((area 2 in figure 3.9). As the user moves through the room, the RSSI values gradually improve, becoming less negative. For example, at grid positions like (3,5) and (4,5), the RSSI is around -20 dBm, indicating the user is getting closer to the tagged object. finally a strong increase near the object ((area 3 in figure 3.9). At position (5,6), where the tagged object is located, there is an intense increase in the RSSI, reaching a value close to 10 dBm, indicating a strong signal and confirming that the object has been located. This demonstrates how the RSSI improves as the user approaches the object. The algorithm successfully guides the user towards the object by detecting stronger RSSI values as the distance between the user and the object decreases.
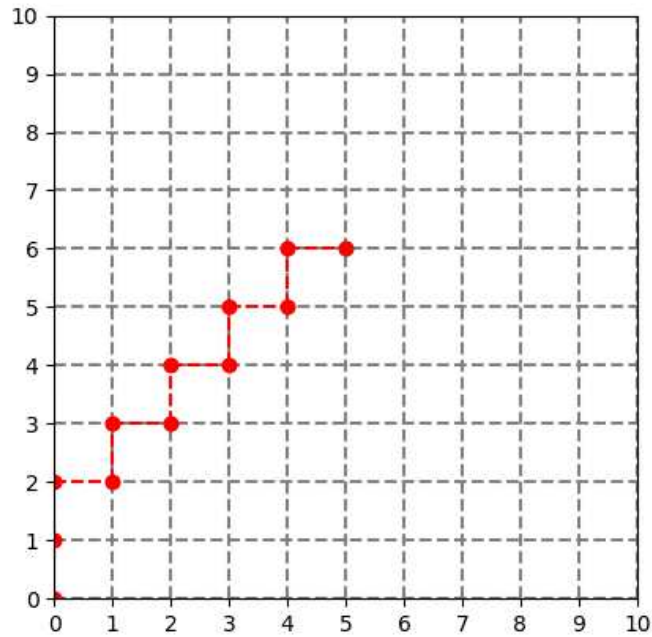
Figure 3.8: Final Path: User Reaches the Object

3.1.5 Limitations and Adaptations

Using the RSSI as a metric for localization in big environments can show several limitations and challenges. While RSSI-based methods can be effective in controlled, small-scale environments like the simulation example, but scaling them to larger environments introduces various complexities. Some of the limitations are :

- Signal Attenuation:
In large environments, the signal weakens especially as the distance between the RFID reader and the tagged object increases. FSPL formula already accounts for signal loss over distance, but in larger environments, this loss can make it difficult to reliably detect objects at far distances.

- Variability: [14]
RSSI is highly sensitive to environmental factors such as walls, furniture, and other obstacles that can cause signal reflections and absorption. These factors are much more noticeable in big environments with varying layouts, leading to unpredictable signal strength readings.

- Multipath Interference :[16]
In larger environments with metallic objects or complex layouts the multipath effects become more and more significant. This happens when the signal bounces off surfaces and reaches the receiver through multiple paths, causing interference. These reflected signals can either strengthen or weaken the perceived signal, leading to inaccurate RSSI readings.

- Reflections and Fading: [25]
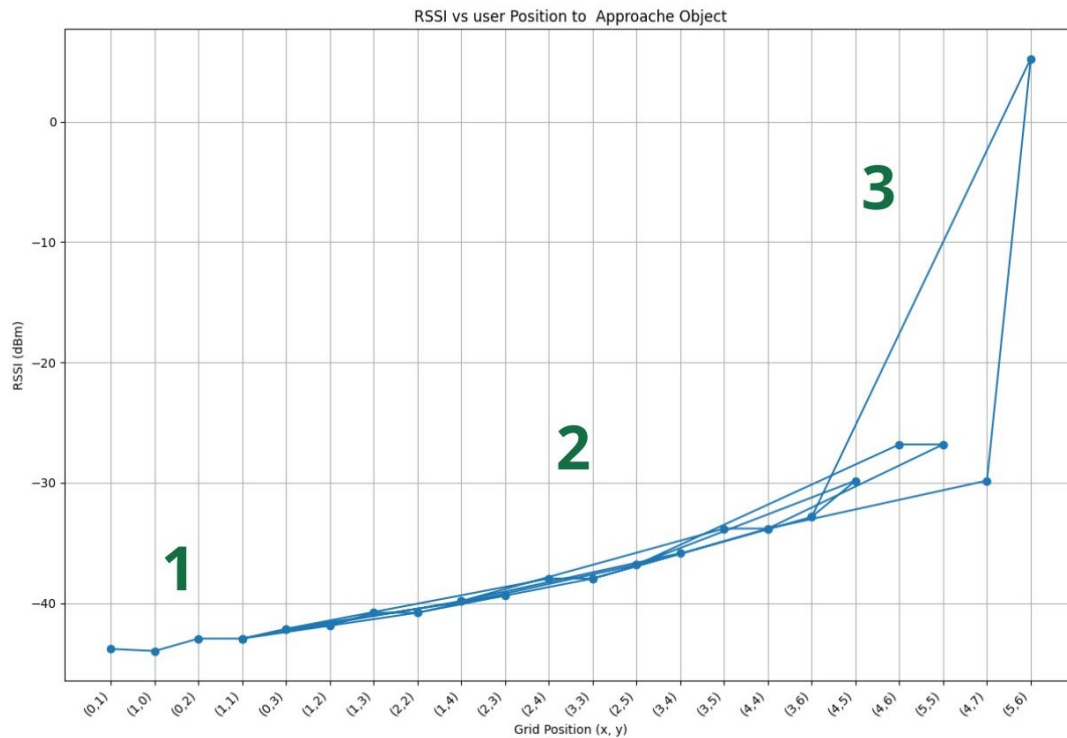
Figure 3.9: RSSI vs the user Position as the user moves to the object

Signal reflections from surfaces like metal or glass can cause a constructive or destructive interference phenomenon, leading to noticeable fluctuations in RSSI values, even when the user is stationary or close to the object.

- Scanning Overhead:

To maintain good accuracy in big spaces, the BFS algorithm or any localization algorithm needs to scan more grid points. The number of positions grows quadratically as the size of the environment increases (for example a 25x25 grid has 625 grid points to analyze). This increases computational overhead and delays in locating the object.

- Multiple Receivers may be needed: [16]

In extensive areas, a single receiver might not be enough. Multiple RFID readers or commentator points like RFID antennas may be needed, however, coordinating multiple readers adds complexity in calibration.

Difficulty in Real-Time Localization :[25]

In larger environments, the time taken for the BFS algorithm to explore all possible points increases, leading to potential latency in real-time localization. The user may need to move around much more to gather reliable RSSI readings, making the process slower and time-consuming.

While RSSI can be a practical and interesting method for localization in small or controlled environments, its accuracy and reliability significantly decrease in larger, more complex environments due to signal attenuation, multipath interference, and environmental variability. To address these challenges, Algorithm B was specifically designed as a more sophisticated solution, incorporating advanced techniques to overcome many of the limitations faced by RSSI-based localization in large-scale or industrial environments.

3.2 Methodology and Development of Algorithm B

Based on the limitations summarized in the previous section, Algorithm A, proved to be insufficient in large or complex environments. While the RSSI-based approach works well in small-scale environments, it faces several important challenges in larger settings. These challenges include signal attenuation, multipath interference, and reflections from surfaces such as walls, floors, and metal objects, which can drastically distort the signal strength measurements. To address these issues, Algorithm B proposes a better and more robust solution, this solution is inspired by the Three-Ray Ground Reflection Model [18], which provides a more accurate representation of signal behavior in environments with multiple reflective surfaces. This model is an extension of the traditional free-space propagation and two-ray models, introducing an additional reflection path from obstacles like walls. As a result, it allows for a more sophisticated key of the multipath propagation effect, which is critical in industrial environments.

3.2.1 Main Concept and Three-Ray Ground Reflection Model Overview

The Three-Ray Ground Reflection Model is an extension of the traditional two-ray model in wireless communication. It is designed to account for the complexity of radio signal propagation in environments where multiple paths can arise due to reflections off surfaces like walls, and obstacles [16].
This modeling is based on Snell's law, the superposition principle, Friis transmission formulation, and analytical geometry for an oblique incidence.[18] It is a powerful method for addressing multipath interference, signal attenuation, and environmental variability. This model is more suited for urban or indoor environments where multiple signal paths are common due to obstacles, such as walls and metallic objects.
The Three-Ray Ground Reflection Model provides a precise definition of radio signal propagation in indoor or urban environments: a signal encounters reflections from both the ground and obstacles such as walls or metal objects, unlike the two-ray model, which only considers the direct path and one ground reflection. This model is particularly useful in environments where multipath interference can significantly impact signal reception.

Figure 3.10 illustrates the propagation of a radio signal based on the Three-Ray Ground Reflection Model, showing three distinct signal paths from a transmitter (Tx) to a receiver (Rx). These paths are defined as follows: The Direct Path (d1): Represented by the pink line, this is the shortest path where the signal travels directly from the transmitter to the receiver without any interference or reflection. The Ground Reflected Path (d2): Represented by the red line, the signal reflects off the floor before reaching the receiver, introducing a phase shift. The Object Reflected Path (d3): Represented by the green line, the signal reflects off an object (such as the roof) before reaching the receiver, making this the longest path.

The combination of these paths results in constructive or destructive interference, depending on the path lengths and phase shifts, which are critical in environments with reflective surfaces.
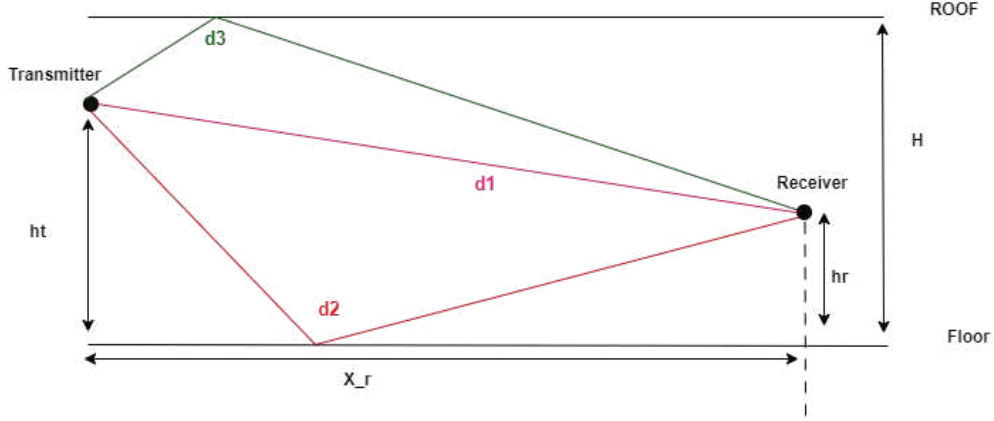
Figure 3.10: Visualization of the Three-Ray Ground Reflection Model Showing Direct, Ground-Reflected, and Object-Reflected Paths

Here, x_r represents the horizontal distance between the transmitter (Tx) and the receiver (Rx). This distance is important as it impacts the calculation of the path lengths (d_1, d_2, and d_3), which in turn affect the overall signal strength and phase at the receiver.

In The Three-Ray model [18], the total electric field $E_{3-\text{ray}}$ at the receiver is the sum of the contributions from the direct path, the ground-reflected path, and an additional object-reflected path, as given by the following equation[18] :

$$E_{3-\text{ray}} = E_1 e^{j\phi_1} + E_2 \Gamma_f e^{j\phi_2} + E_3 \Gamma_c e^{j\phi_3} \tag{3.4}$$

Where:

- E_1, E_2, and E_3 represent the electric field amplitudes of the direct, ground-reflected, and object-reflected paths, respectively.

- ϕ_1, ϕ_2, and ϕ_3 are the phase shifts corresponding to the direct, ground-reflected, and object-reflected paths, respectively.

- Γ_f and Γ_c are the reflection coefficients for the floor and the ceiling (or object), respectively.

The phase differences between the direct path and the reflected paths are computed as:

$$\Delta\phi_f = \frac{2\pi}{\lambda}(d_2 - d_1), \quad \Delta\phi_c = \frac{2\pi}{\lambda}(d_3 - d_1) \tag{3.5}$$

Where d_1, d_2, and d_3 are the path lengths of the direct, ground-reflected, and object-reflected rays, respectively, given by:

35

$$d_1 = \sqrt{x_r^2 + (h_t - h_r)^2} \tag{3.6}$$

$$d_2 = \sqrt{x_r^2 + (h_t + h_r)^2} \tag{3.7}$$

$$d_3 = \sqrt{x_r^2 + (2H - h_t - h_r)^2} \tag{3.8}$$

Where:

- x_r is the horizontal distance between the transmitter and receiver.

- h_t and h_r are the heights of the transmitter and receiver, respectively.

- H is the height of the room or obstacle from which the signal reflects.

The total received power $P_{r,3-\text{ray}}$ can be derived from the magnitude of the electric field:

$$P_{r,3-\text{ray}}(x_r) = \frac{|E_{3-\text{ray}}|^2}{2\eta_0} \tag{3.9}$$

Where η_0 is the intrinsic impedance of free space. The path loss in the three-ray model, $PL_{3-\text{ray}}$, is then given by:

$$PL_{3-\text{ray}}(x_r) = 10\log_{10}\left(\frac{P_{r,3-\text{ray}}(x_r)}{P_t}\right) \tag{3.10}$$

Where P_t is the transmitted power. This model incorporates the effects of multipath reflections and provides a more accurate representation of signal attenuation in complex environments, particularly for indoor settings with multiple reflective surfaces.

3.2.2   Proposed Solution: Localization Using the Three-Ray Ground Reflection Model

In light of the limitations identified in the previous approach, particularly the challenges associated with using RSSI-based localization methods in large and complex environments, I developed an advanced solution leveraging the Three-Ray Reflection Model. This model addresses the issues of signal attenuation, multipath interference, and reflections, which are critical factors in environments such as warehouses, where metal creates significant challenges for signal propagation.

The image 3.11 represents a practical scenario of RFID signal propagation in a room. A user is equipped with a tablet with an RFID reader, while a metallic tagged object is located in the middle of the room. The user is trying to locate the toolbox by analyzing the RFID signal paths. Three distinct signal paths are shown:

- Direct Path (d_1)
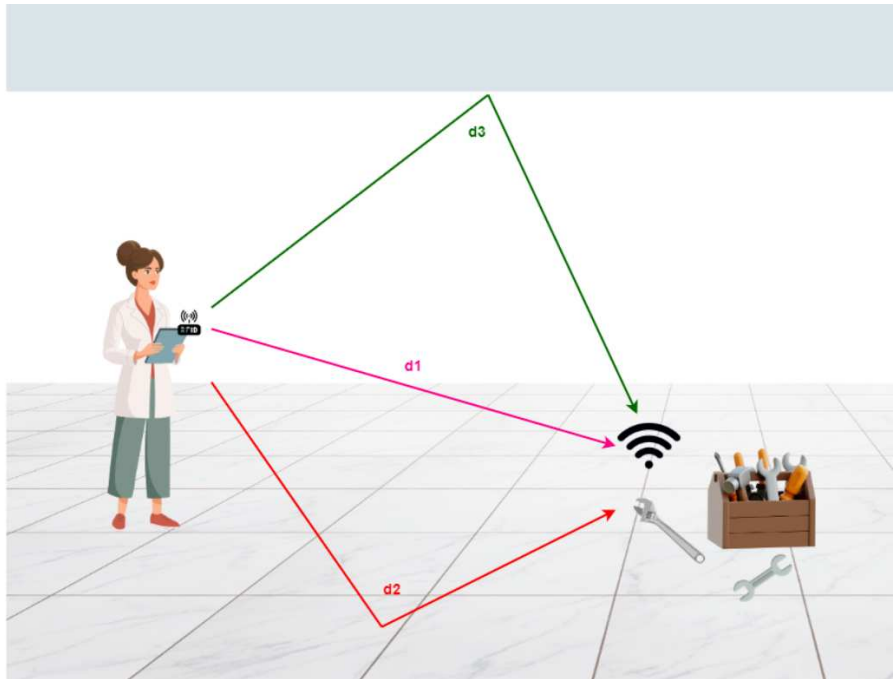
Figure 3.11: Signal Propagation Visualization based on the Three-Ray Reflection Model: Direct, Ground-Reflected, and Object-Reflected Paths

The signal travels directly from the RFID reader held by the user to the RFID tag attached to the object. This is the shortest and most straightforward path between the transmitter (reader) and the target (tag). In this scenario, d_1 represents the distance where no reflections occur.

- Direct Path (d_2)

The signal is transmitted from the RFID reader, reflects off the ground, and then reaches the RFID tag on the object. This path is longer than d_1 because the signal travels from the reader to the ground, bounces off the surface, and then continues to the tag. The reflection introduces a phase shift and attenuation, making this path more complex than the direct path.

- Direct Path (d_3)

The signal is transmitted from the RFID reader and reflects off an overhead object, such as the roof before reaching the RFID tag. This is the longest of the three paths because the signal must travel from the reader to the reflecting interface and then to the tag. The longer distance causes the signal to experience further attenuation and phase shifts.

To fully understand the behavior of the RFID signal in Figure 3.11), we must analyze the paths d_1, d_2, and d_3 using principles of trigonometry. The visualization shows that the RFID reader sends signals that travel along multiple paths one directly to the RFID tag and others through reflections from the ground or the roof. To quantify these variations, we can model the system geometrically. In the second image (Figure 3.12), the relationship between the RFID reader, tag, and reflected objects is expressed as a series of triangles. By applying trigonometric principles such as the Pythagorean theorem, we can calculate the exact distances for each path d_1, d_2, and d_3.

d_1 is the shortest, representing the direct line between the reader and the tag, forming a right triangle where the horizontal distance is x_r and the vertical distance is the height difference between the reader and tag. The paths d_2 and d_3 involve reflections, and thus require additional complex geometric analysis, as they form triangles with additional distances caused by the reflection points.

By applying triangle similarity and the Pythagorean theorem, we can derive equations for these paths that allow us to understand signal behavior in this multipath environment. The following part, will focus on this geometric model in detail and explain how these calculations help predict signal strength and interference for RFID-based localization systems.

Trigonometric Analysis of the Signal Paths

- Tx: The RFID reader, positioned at coordinates $(0, h_t, 0)$, where h_t is the height of the transmitter (user with RFID reader).

- Rx: The RFID tag attached to the object, positioned at coordinates $(x_r, h_r, 0)$, where x_r is the horizontal distance between the reader and tag, and h_r is the height of the receiver (tagged object).

- $(x_2, 0, 0)$: The point of reflection on the ground, where the signal reflects and then reaches the receiver. This point lies at x_2 along the horizontal axis.

- $(x_3, H, 0)$: The point of reflection on the roof, where the signal reflects off an overhead object. The height of the ceiling is H.

And for the distance hey are defined :
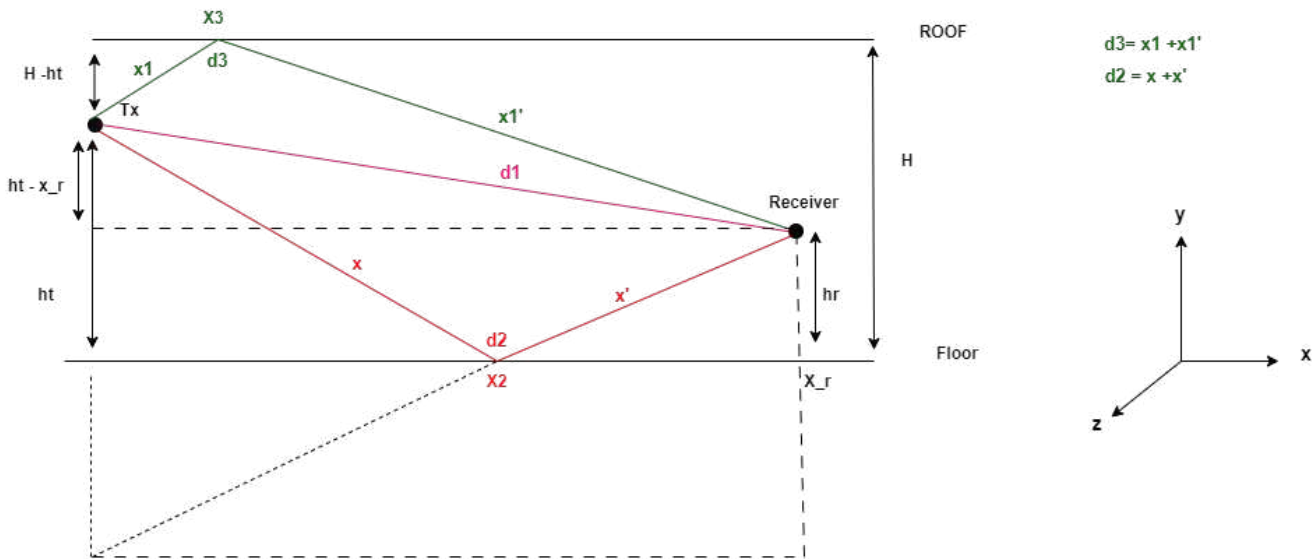
Figure 3.12: Geometric Representation of Signal Paths

- d_1: The Direct Path between the reader and the tag. This is the **line-of-sight (LoS) distance**, where no reflections occur.

- d_2: The Ground-Reflected Path, where the signal reflects off the ground. This is a **non-line-of-sight (NLoS)) path.**

- d_3: The Object-Reflected Path, where the signal reflects off the ceiling. This is also a **NLoS) path.**

We can use the concept of similar triangles to find relationships between the horizontal distances and the heights of the transmitter, receiver, and reflection points. By analyzing the triangles formed by the direct, ground-reflected, and object-reflected paths, we can calculate important proportions that help determine the distances each signal travels along these paths. From the triangle similarity, we can derive the following relations :

$$\frac{x_r}{h_t + h_r} = \frac{x_2}{h_t}$$

This equation expresses the ratio of the total horizontal distance (x_r) to the total height ($h_t + h_r$) compared to the horizontal distance to the ground-reflection point (x_2) and the height of the transmitter (h_t).

For the object-reflected path, we have:

$$x_3 = \frac{H - h_t}{2H - h_r - h_t} \cdot x_r$$

Here, x_3 is the horizontal distance along the object-reflected path, taking into account the height of the ceiling (H), the height of the transmitter (h_t), and the height of the receiver (h_r).

Calculating d_1, d_2, and d_3 Using the Pythagorean Theorem by applying the Pythagorean theorem to calculate the lengths of each path.

39

- Direct Path d_1: The shortest path, where the signal travels directly from the transmitter to the receiver.

$$d_1 = \sqrt{x_r^2 + (h_t - h_r)^2}$$

- Ground-Reflected Path d_2: the signal reflects off the ground

$$d_2 = \sqrt{x_r^2 + (h_t + h_r)^2}$$

- Object-Reflected Path d_3:
$$d_3 = \sqrt{x_r^2 + (2H - h_t - h_r)^2}$$

Calculation of the Ground-Reflected NLoS Path Distance
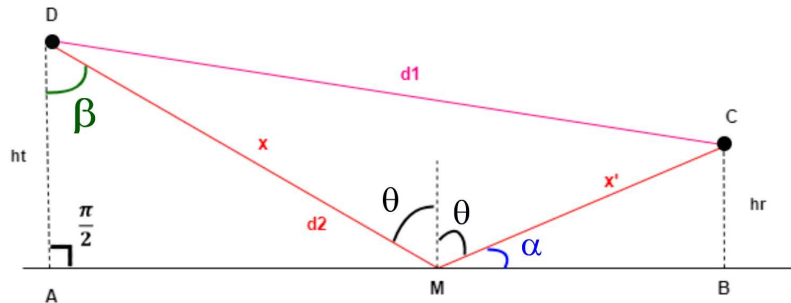
Figure 3.13: Geometric Representation of Signal Paths

To better understand how the signal propagates in the environment, we study the geometric relationships between the RFID reader and the RFID tags to determine the phase difference.

This image 3.13 illustrates this geometric relationship. The paths labeled d_1 and d_2 represent the direct path or Los path and the ground-reflected path or one of the 2 Nlos paths. The angles involved in the geometry of the signal paths are important for understanding the relationships between the heights and horizontal distances. The image highlights the following key points and distances:

we define the angles in the figure 3.13:

- **Angle α**: The angle between the ground and the line connecting the RFID reader (Tx) and the ground reflection point M, represented in blue.

- **Angle θ**: The angle of incidence and reflection at point M. The angles of incidence and reflection are equal, as shown in black.

- **Angle β**: The angle between the vertical line at point D and the direct path d_1, which connects point D (on the reader's vertical axis) to point C (on the receiver's vertical axis). This angle is represented in green.

We define the distance :

- d_1: The Los path distance

- d_2: One of the Nlos path distance

To accurately describe the behavior of the signal propagation paths, we apply fundamental trigonometric principles to the geometric relationships between the RFID reader, the RFID tag, and the reflection points. By leveraging triangle similarity and using the Law of Cosines (al-Kashi's theorem), we were able to establish precise mathematical formulas that express the relationships between the heights of the reader and tag, the horizontal distances between key points, and the angles of incidence and reflection. In the following sections, we will carry out the calculations to find the phase difference. These relationships are essential for calculating the exact path lengths and phase differences in direct and ground-reflected signal paths.

So the first 2 relations are from the triangle similarity:

$$\sin \alpha = \frac{h_t}{DM}$$

$$\sin \alpha = \frac{h_r}{MC}$$

Where:

- DM is the slant distance from point A to the reflection point M.

- MC is the slant distance from point M to the receiver.

- h_r is the height of the RFID tag.

- h_t is the height of the RFID reader.

Applying the Law of Cosines or al-Kashi's theorem in Triangle DMC:

$$DC^2 = DM^2 + MC^2 - 2 \cdot DM \cdot MC \cdot \cos(2\alpha) \tag{3.11}$$

- Calculation of DC^2 Using the Law of Cosines

We start by expressing DM and MC in terms of the horizontal distances x and x' as mentioned in 3.13 as follows:

$$DM = \frac{h_t}{\sin \alpha} = \sqrt{x^2 + h_t^2}$$

$$MC = \frac{h_r}{\sin \alpha} = \sqrt{x'^2 + h_r^2}$$

- x is the horizontal distance between the transmitter (Tx) and the ground reflection point M, and h_t is the height of the RFID reader.

- x' is the horizontal distance between point M and receiver (Rx) , and h_r is the height of the RFID tag.

Next, we use the trigonometric identity for $\cos(2\alpha)$:

$$\cos(2\alpha) = \cos^2(\alpha) - \sin^2(\alpha) = 1 - 2\sin^2(\alpha)$$

Now, applying the Law of Cosines in triangle DMC, we can write:

$$DC^2 = DM^2 + MC^2 - 2 \cdot DM \cdot MC \cdot \cos(2\alpha)$$

Substituting $DM = \frac{h_t}{\sin\alpha}$ and $MC = \frac{h_r}{\sin\alpha}$ into the equation, we get:

$$DC^2 = \left(\frac{h_t}{\sin\alpha}\right)^2 + \left(\frac{h_r}{\sin\alpha}\right)^2 - 2 \cdot \frac{h_t}{\sin\alpha} \cdot \frac{h_r}{\sin\alpha} \cdot \cos(2\alpha)$$

Using the trigonometric identity $\cos(2\alpha) = 1 - 2\sin^2(\alpha)$, we can substitute this into the equation:

$$DC^2 = \frac{h_t^2}{\sin^2\alpha} + \frac{h_r^2}{\sin^2\alpha} - 2 \cdot \frac{h_t \cdot h_r}{\sin^2\alpha} \cdot (1 - 2\sin^2(\alpha))$$

Now expanding the equation:

$$DC^2 = \frac{h_t^2}{\sin^2\alpha} + \frac{h_r^2}{\sin^2\alpha} - 2 \cdot \frac{h_t \cdot h_r}{\sin^2\alpha} + 4 \cdot \frac{h_t \cdot h_r}{\sin^2\alpha} \cdot \sin^2(\alpha)$$

$$DC^2 = \frac{1}{\sin^2\alpha} \left(h_t^2 + h_r^2 - 2 \cdot h_t \cdot h_r \cdot (1 - 2\sin^2(\alpha))\right)$$

Thus, the final expression for DC^2 is:

$$DC^2 = \frac{1}{\sin^2\alpha} \left(h_t^2 + h_r^2 - 2 \cdot h_t \cdot h_r + 4 \cdot h_t \cdot h_r \cdot \sin^2(\alpha)\right)$$

We define DC^2 as d^2, the LoS distance we are trying to find. Thus, this expression represents d^2 in terms of the heights h_t, h_r, and the angle α, where d is the line-of-sight (LoS) distance.

Substitute $X = \sin\alpha$ into the equation:

$$d^2 = \frac{1}{X^2} \left(h_t^2 + h_r^2 - 2 \cdot h_t \cdot h_r + 4 \cdot h_t \cdot h_r \cdot X^2\right)$$

We multiply both sides of the equation by X^2 to simplify:

$$d^2 \cdot X^2 = h_t^2 + h_r^2 - 2 \cdot h_t \cdot h_r + 4 \cdot h_t \cdot h_r \cdot X^2$$

Thus, the equation becomes:

$$d^2 \cdot X^2 = h_t^2 + h_r^2 - 2 \cdot h_t \cdot h_r + 4 \cdot h_t \cdot h_r \cdot X^2$$

Factor out X^2 from the left-hand side:

$$X^2 \left(d^2 - 4 \cdot h_t \cdot h_r\right) = h_t^2 + h_r^2 - 2 \cdot h_t \cdot h_r$$

Finally, solve for X^2:

$$X^2 = \frac{h_t^2 + h_r^2 - 2 \cdot h_t \cdot h_r}{d^2 - 4 \cdot h_t \cdot h_r}$$

$$X^2 = \frac{(h_t - h_r)^2}{d^2 - 4 \cdot h_t \cdot h_r}$$

Or $X = \sin \alpha$

$$\sin^2 \alpha = \frac{(h_t - h_r)^2}{d^2 - 4 \cdot h_t \cdot h_r}$$

$$\alpha = \arcsin \left(\sqrt{\frac{(h_t - h_r)^2}{d^2 - 4 \cdot h_t \cdot h_r}} \right)$$

To ensure that the inverse sine function $\arcsin$ is valid, the argument inside the function must lie within the range $[-1, 1]$. This imposes the condition:

$$-1 \leq \sqrt{\frac{(h_t - h_r)^2}{d^2 - 4 \cdot h_t \cdot h_r}} \leq 1$$

We can now express the distances DM and MC in terms of the heights and the angle α as follows:

$$DM = \frac{h_t}{\sin \alpha} = x$$

$$MC = \frac{h_r}{\sin \alpha} = x'$$

Thus, we have:

$$x = \frac{h_t}{\sin \alpha}, \quad x' = \frac{h_r}{\sin \alpha}$$

$$X = \frac{h_t \cdot \sqrt{d^2 + 4 \cdot h_t \cdot h_r}}{h_t + h_r}, X' = \frac{h_r \cdot \sqrt{d^2 + 4 \cdot h_t \cdot h_r}}{h_t + h_r}$$

$$X + X' = \frac{h_t \cdot \sqrt{d^2 + 4 \cdot h_t \cdot h_r}}{h_t + h_r} + \frac{h_r \cdot \sqrt{d^2 + 4 \cdot h_t \cdot h_r}}{h_t + h_r}$$

These distances, x and x', represent the horizontal components of the first non-line-of-sight (NLoS) distances in the signal propagation model.

- Path-Length Difference and Phase Difference

The path-length difference $\Delta d_{3\_ray\_model}$ between the reflected and direct paths can be expressed as:

$$\Delta d_{3\_ray\_model} = x + x' - d_1 = \frac{\sqrt{d^2 + 4 \cdot h_t \cdot h_r} \cdot (h_t + h_r)}{h_t + h_r} - d_1$$

43

Where d_1 is the direct line-of-sight (LoS) as we mentioned before :

$$d_1 = \sqrt{(h_t - h_r)^2 + d^2}$$

$$\Delta d_{3\_ray\_model} = \sqrt{d^2 + 4 \cdot h_t \cdot h_r} - \sqrt{(h_t - h_r)^2 + d^2}$$

Next, we calculate the phase difference $\Delta\phi_{3\_ray\_model}$, which is given by:

$$\Delta\phi_{3\_ray\_model} = \frac{2\pi \Delta d_{3\_ray\_model}}{\lambda}$$

Substituting the expression for $\Delta d_{3\_ray\_model}$, we get:

$$\Delta\phi_{3\_ray\_model} = \frac{2\pi}{\lambda} \left(\sqrt{d^2 + 4 \cdot h_t \cdot h_r} - \sqrt{(h_t - h_r)^2 + d^2} \right)$$

- Why the Approximation is Not Used

If we were to use the Taylor series approximation in our solution, the path-length difference Δd between the direct and reflected paths would be simplified $d \gg (h_t + h_r)$.

The exact path-length difference is given by:

$$\Delta d = \sqrt{(h_t + h_r)^2 + d^2} - \sqrt{(h_t - h_r)^2 + d^2}$$

To apply the Taylor series approximation, we expand both square roots around $d \gg (h_t + h_r)$, using the first few terms of the series. For a square root $\sqrt{1 + x}$, the Taylor expansion is:

$$\sqrt{1 + x} \approx 1 + \frac{x}{2} - \frac{x^2}{8} + \dots$$

Applying this expansion to both terms in Δd:

$$\sqrt{(h_t + h_r)^2 + d^2} \approx d \left(1 + \frac{(h_t + h_r)^2}{2d^2} \right)$$

$$\sqrt{(h_t - h_r)^2 + d^2} \approx d \left(1 + \frac{(h_t - h_r)^2}{2d^2} \right)$$

Now, subtracting the two expressions gives the simplified path-length difference:

$$\Delta d \approx d \left(\frac{(h_t + h_r)^2}{2d^2} - \frac{(h_t - h_r)^2}{2d^2} \right)$$

Simplifying further:

$$\Delta d \approx \frac{2h_t h_r}{d}$$

However, in environments like warehouses, the signal is likely to encounter multiple reflections from nearby surfaces such as walls, floors, shelves, and other obstacles. These reflections introduce multipath effects, causing phase shifts, interference, and signal attenuation, in this situation the Taylor series approxi-

mation used in the two-ray model fails to accurately capture this complexity. This approximation simplifies the path-length difference between the direct and reflected signals by assuming $d \gg (h_t + h_r)$, which is not realistic in a warehouse setting.

Calculating the roof-reflected NLoS distance
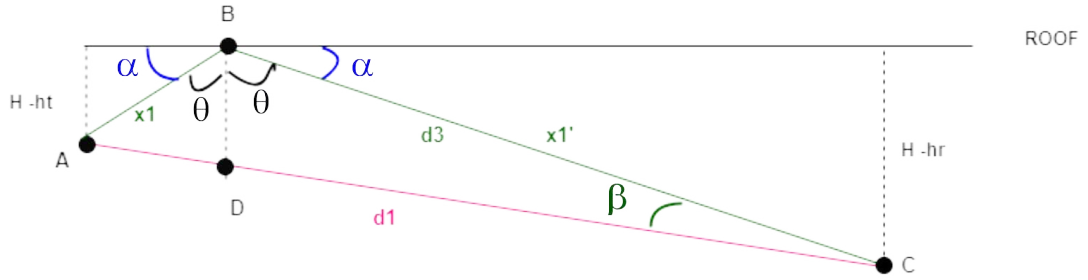
Figure 3.14: Geometric Representation of one Direct and roof-Reflected Signal Paths

To calculate the roof-reflected NLoS distance, we apply a similar process to the one used for the ground-reflected NLoS distance. In this case, the signal reflects off the roof before reaching the receiver. This is the trigonometric relations used to find the reflection point on the roof and the associated distances:

$$\sin \alpha = \frac{H - h_r}{CB}, \quad \sin \alpha = \frac{H - h_t}{AB}$$

Where:

- $AB = x_1$: The horizontal distance between the transmitter (Tx) and the reflection point on the roof.

- $CB = x_1'$: The horizontal distance between the reflection point on the roof and the receiver (Rx).

- α: The angle between the roof and the path to the receiver.

Using al-Kashi's theorem (Law of Cosines) in triangle ABC, we can express the roof-reflected NLoS path distance d_3 as follows:

$$AC^2 = AB^2 + BC^2 - 2 \cdot AB \cdot BC \cdot \cos(\beta)$$

Where:

- $AB = x_1$,

- $BC = x_1'$,

- β is the angle between the paths AB and BC, related to the reflection point on the roof.

Substituting:

$$BC = \frac{H - h_r}{\sin \alpha}, \quad AB = \frac{H - h_t}{\sin \alpha}$$

45

into the Law of Cosines formula for triangle ABC, we get:

$$AC^2 = \left(\frac{H-h_t}{\sin\alpha}\right)^2 + \left(\frac{H-h_r}{\sin\alpha}\right)^2 - 2\cdot\frac{H-h_t}{\sin\alpha}\cdot\frac{H-h_r}{\sin\alpha}\cdot\cos(\beta)$$

We can simplify by factoring out $\frac{1}{\sin^2\alpha}$:

$$AC^2 = \frac{1}{\sin^2\alpha}\left((H-h_t)^2 + (H-h_r)^2 - 2\cdot(H-h_t)\cdot(H-h_r)\cdot\cos(\beta)\right)$$

Thus, the final expression for the roof-reflected NLoS distance AC is:

$$AC^2 = \frac{1}{\sin^2\alpha}\left((H-h_t)^2 + (H-h_r)^2 - 2\cdot(H-h_t)\cdot(H-h_r)\cdot\cos(\beta)\right)$$

Thus, the final expression for the roof-reflected NLoS distance AC is:

$$AC^2 = \frac{1}{\sin^2\alpha}\left((H-h_t)^2 + (H-h_r)^2 - 2\cdot(H-h_t)\cdot(H-h_r) + 4\cdot(H-h_t)\cdot(H-h_r)\cdot\sin^2(\alpha)\right)$$

We define DC^2 as d^2, the LoS distance we are trying to find. Thus, this expression represents d^2 Substitute X = sin α into the equation:

$$d^2\cdot X^2 = (H-h_t)^2 + (H-h_r)^2 - 2\cdot(H-h_t)\cdot(H-h_r) + 4\cdot(H-h_t)\cdot(H-h_r)\cdot X^2$$

And solving for X^2 to find the expression of $sin(\alpha)$ we get :

$$\sin\alpha = X = \sqrt{\frac{(H-h_t)^2 + (H-h_r)^2 - 2\cdot(H-h_t)\cdot(H-h_r)}{d^2 - 4\cdot(H-h_t)\cdot(H-h_r)}}$$

We can substitute this expression into the formulas for BC and AB we get:

$$BC = \frac{(H-h_r)\cdot\sqrt{d^2 - 4\cdot(H-h_t)\cdot(H-h_r)}}{\sqrt{(H-h_t)^2 + (H-h_r)^2 - 2\cdot(H-h_t)\cdot(H-h_r)}}$$

$$AB = \frac{(H-h_t)\cdot\sqrt{d^2 - 4\cdot(H-h_t)\cdot(H-h_r)}}{\sqrt{(H-h_t)^2 + (H-h_r)^2 - 2\cdot(H-h_t)\cdot(H-h_r)}}$$

- Path-Length Difference and Phase Difference The path-length difference Δd between the reflected and direct paths can be expressed as:

$$\Delta d = x_1 + x_1' - d_3$$

while for the previous equations, we have

$$AB = x_1, BC = x_1'$$

We define :

$$\Delta d = \frac{(H - h_t) \cdot \sqrt{d^2 - 4 \cdot (H - h_t) \cdot (H - h_r)}}{\sqrt{(H - h_t)^2 + (H - h_r)^2 - 2 \cdot (H - h_t) \cdot (H - h_r)}}$$
$$+ \frac{(H - h_r) \cdot \sqrt{d^2 - 4 \cdot (H - h_t) \cdot (H - h_r)}}{\sqrt{(H - h_t)^2 + (H - h_r)^2 - 2 \cdot (H - h_t) \cdot (H - h_r)}}$$
$$- \sqrt{(h_t - h_r)^2 + d^2}$$

Factor out the common term:

$$\Delta d = \frac{\sqrt{d^2 - 4 \cdot (H - h_t) \cdot (H - h_r)} \cdot ((H - h_t) + (H - h_r))}{\sqrt{(H - h_t)^2 + (H - h_r)^2 - 2 \cdot (H - h_t) \cdot (H - h_r)}} - \sqrt{(h_t - h_r)^2 + d^2}$$

Next, we calculate the phase difference $\Delta\phi$, which is given by:

$$\Delta\phi = \frac{2\pi\Delta d}{\lambda}$$

Substituting the expression for Δd, we get:

$$\Delta\phi = \frac{2\pi}{\lambda} \left(\frac{\sqrt{d^2 - 4 \cdot (H - h_t) \cdot (H - h_r)} \cdot ((H - h_t) + (H - h_r))}{\sqrt{(H - h_t)^2 + (H - h_r)^2 - 2 \cdot (H - h_t) \cdot (H - h_r)}} - \sqrt{(h_t - h_r)^2 + d^2} \right)$$

Where:

- Δd is the path-length difference,

- λ is the wavelength of the signal,

- H is the height of the reflecting roof,

- h_t is the height of the transmitter,

- h_r is the height of the receiver,

- d is the horizontal distance between the transmitter and the receiver.

3.2.3 Localization Using the Five-ray Ground Reflection Model

To comprehensively understand the signal propagation in an enclosed environment, we tried to explore further the 5-ray model as illustrated in figure 3.15. In contrast to simpler models like the 2-ray or 3-ray models, which consider only a few signal reflection paths, the 5-ray model will consider the complex interaction of the RFID signal with the surrounding elements. Specifically, it considers reflections from the floor, roof, and two sidewalls in addition to the direct line-of-sight (LOS) path between the RFID reader and the tagged object. The key idea of the 5-ray model is that in an indoor environment, the signal will not follow a direct path only but also encounter multiple obstacles. These obstacles cause the signal to reflect in different directions, creating multiple paths of varying lengths. Each of these paths introduces a phase

shift, changes in signal strength, and potential interference. By incorporating five distinct paths the model captures the complexity of real-world signal conduct in such environments and takes into consideration the multipath problem. This enables us to predict how the signal will behave more accurately and what phase differences and propagation delays will occur. The 5-ray model thus helps to address challenges like multipath interference, providing a more reliable framework for analyzing and optimizing RFID-based localization in complex, enclosed spaces.
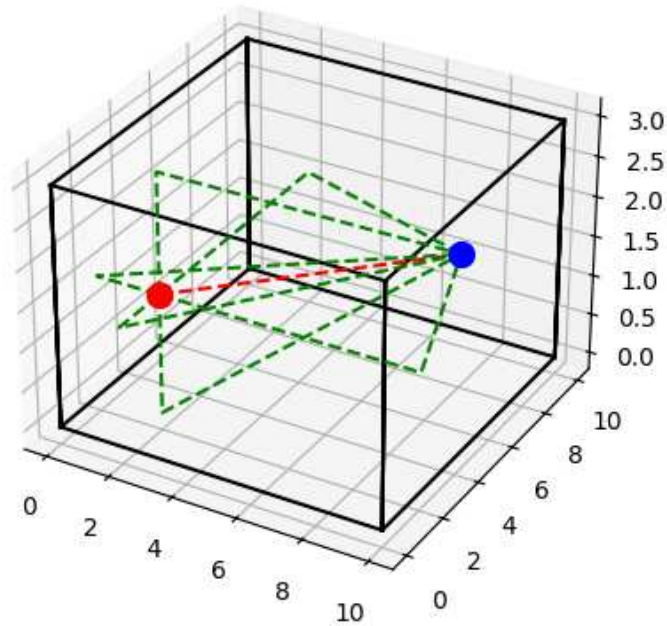
Figure 3.15: 3D Visualization of 5-Ray Signal Propagation with Reflections in an Enclosed Environment

In our second scenario, shown in figure 3.16, the transmitter is positioned in one corner of the room, and the receiver is located at another point. The lines represent the indirect paths where the signal undergoes reflections off different surfaces (floor, walls, ceiling) before reaching the receiver. These multiple paths introduce delays, phase shifts, and interference, which need to be accounted for while we are trying to localize the tagged object. This visualization represents the complexity of signal propagation in an indoor environment, making the 5-ray model a more accurate representation of real-world scenarios in an industrial environment.

- d (green): The direct line-of-sight (LoS) path between the transmitter (Tx) and the receiver (Rx).

- d_1 (pink): The path reflected off the wall 1.

- d_2 (black): The path reflected off the wall 2.

- d_4 (yellow): The path reflected off the floor.
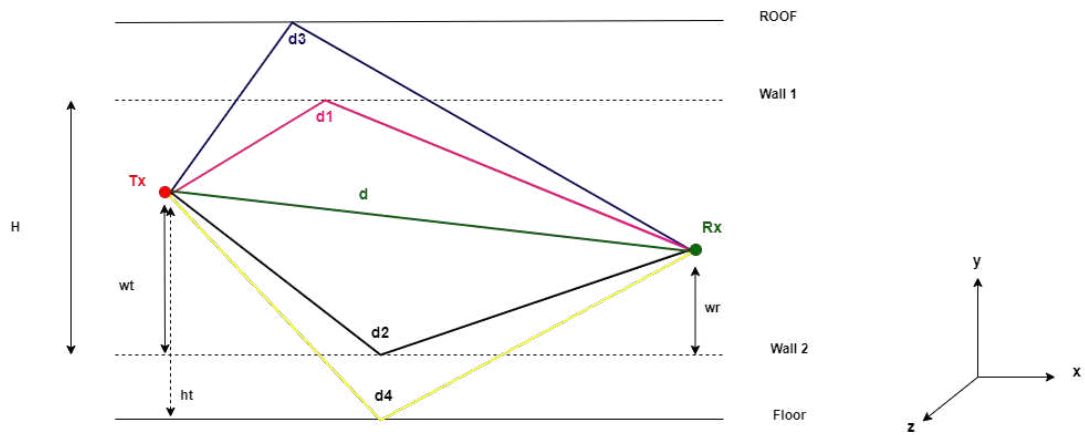
Figure 3.16: 2D Representation of the 5-Ray Propagation Model: Direct and Reflected Signal Paths
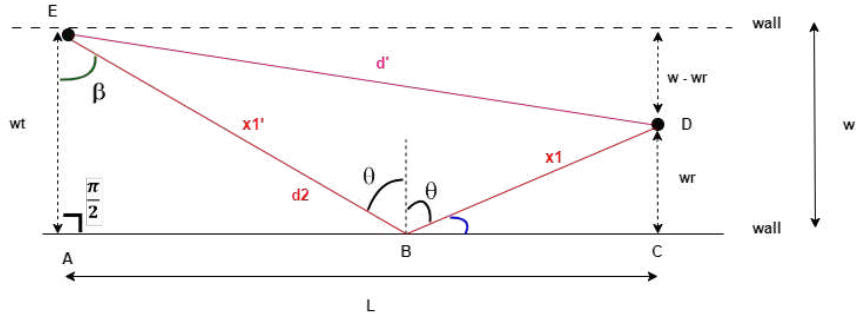
- d_3 (blue): The path reflected off the ceiling.

Figure 3.17: This figure illustrates the first direct and NLoS signal paths, reflected from the wall, as part of the 5-ray model. The distances w_r and w_t represent the distances from the receiver and transmitter to the wall, respectively. L is the room width.

Calculation of the Wall-Reflected NLoS Distance

To simplify the analysis of the 5-ray propagation model (as shown in the model in figure 3.16), we divide it into two separate 3-ray models. By breaking down the more complex 5-ray model into these smaller segments, we can better analyze the individual contributions of each reflection to the overall signal propagation. In the next section, we will calculate the effects of the reflections from the walls as shown in figure 3.17, analyzing how these surfaces contribute to the phase shifts, signal attenuation, and path-length differences. This approach enables us to comprehensively understand how each boundary affects the RFID signal behavior in an enclosed space. To calculate the Non-Line-of-Sight (NLoS) distance for the signal path reflected off the wall, we use a similar approach to that of the ground-reflected and roof-reflected paths. In this case, the signal is reflected off the wall before reaching the receiver.

The total NLoS distance we are looking for is $EB + BD$, where E and B are the reflection points.

First, we define the trigonometric relationships for the angle α:

$$\sin \alpha = \frac{w_r}{BD}, \quad \sin \alpha = \frac{w_t}{EB}$$

Where:

- w_r is the distance between the receiver and the wall,

- w_t is the distance between the transmitter and the wall,

- BD and EB are the horizontal components of the reflection path.

Using Al-Kashi's theorem (Law of Cosines) in the triangle EBD, we can write the total NLoS distance as:

$$ED^2 = EB^2 + BD^2 - 2 \cdot EB \cdot BD \cdot \cos(2\theta)$$

Where:

- $ED = d$: The total NLoS path distance,

- EB and BD : The horizontal reflection path distances,

50

- θ: The angle of incidence/reflection at the wall.

Using the trigonometric identity, we can substitute into the equation to get:

$$ED^2 = EB^2 + BD^2 - 2 \cdot EB \cdot BD \cdot (1 - 2\sin^2(\alpha))$$

Or in the triangle EBD

$$\cos(2\theta) = \cos(\pi - 2\alpha) = -\cos(2\alpha) = -(1 - 2\sin^2(\alpha))$$

$$ED^2 = \left(\frac{w_t}{\sin\alpha}\right)^2 + \left(\frac{w_r}{\sin\alpha}\right)^2 + 2 \cdot \frac{w_t}{\sin\alpha} \cdot \frac{w_r}{\sin\alpha} \cdot (1 - 2\sin^2(\alpha))$$

$$ED^2 = \frac{1}{\sin^2\alpha}\left(w_t^2 + w_r^2 + 2 \cdot w_t \cdot w_r - 4\sin^2(\alpha) \cdot w_t \cdot w_r\right)$$

Thus, the final expression for the NLoS distance d is:

$$d^2 = \frac{1}{\sin^2\alpha}\left(w_t^2 + w_r^2 + 2 \cdot w_t \cdot w_r - 4\sin^2(\alpha) \cdot w_t \cdot w_r\right)$$

Now let's substitute $\sin(\alpha) = x$:

$$d^2 = \frac{1}{x^2}\left(w_t^2 + w_r^2 + 2 \cdot w_t \cdot w_r - 4 \cdot x^2 \cdot w_t \cdot w_r\right)$$

Now, solve for x^2:

$$x^2 = \frac{w_t^2 + w_r^2 + 2 \cdot w_t \cdot w_r}{d^2 + 4 \cdot w_t \cdot w_r}$$

Thus, the value of x is:

$$x = \sqrt{\frac{w_t^2 + w_r^2 + 2 \cdot w_t \cdot w_r}{d^2 + 4 \cdot w_t \cdot w_r}}$$

$$x = \sqrt{\frac{(w_t + w_r)^2}{d^2 + 4 \cdot w_t \cdot w_r}}$$

so we have finally,

$$BD = \frac{w_r \cdot \sqrt{d^2 + 4 \cdot w_t \cdot w_r}}{w_t + w_r}, \quad EB = \frac{w_t \cdot \sqrt{d^2 + 4 \cdot w_t \cdot w_r}}{w_t + w_r}$$

As mentioned in the 5-ray propagation model, the signal is subject to multiple reflections. Unlike simpler models that only account for single reflections, the 5-ray model considers the double reflection effect caused by both side walls. This means that the signal may reflect off one wall, and simultaneously reflect again off the opposite wall before reaching the receiver. These additional reflections introduce more complexity into the model, as each wall reflection leads to additional changes in the signal path length and phase. The

combined effect of these double reflections needs to be accurately modeled to predict the behavior of the signal in warehouses. Accounting for these double-wall reflections helps improve the accuracy of the RFID localization system.
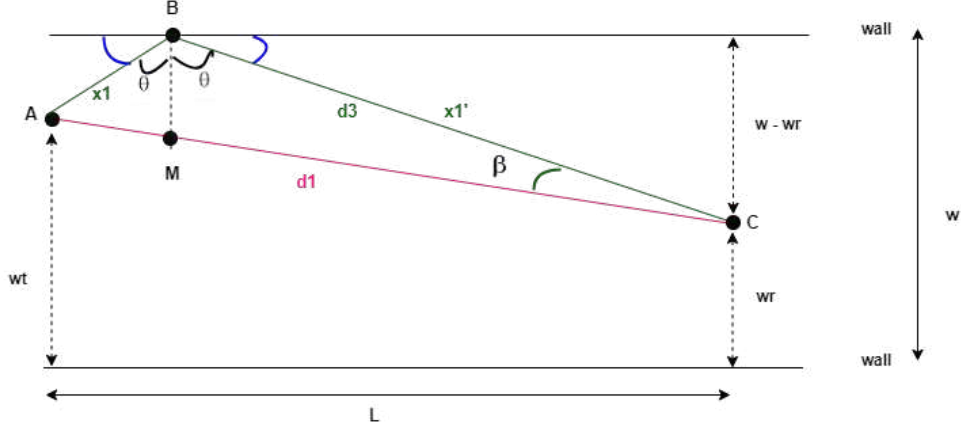
Figure 3.18: This figure illustrates the first direct and the second NLoS signal paths, reflected from the wall, as part of the 5-ray model. The distances w_r and w_t represent the distances from the receiver and transmitter to the wall, respectively. L is the room width.

In this figure, we calculate the second wall-reflected NLoS path distance, denoted as d_3, based on the geometric relationships between the transmitter (Tx), the receiver (Rx), and the reflection point on the wall.

We have the following trigonometric relationships for the reflection points:

$$\sin \alpha = \frac{w - w_t}{AB}, \quad \sin \alpha = \frac{w - w_r}{BC}$$

Where:

- $AB = x$: The horizontal distance between the transmitter and the wall reflection point.

- $BC = x'$: The horizontal distance between the wall reflection point and the receiver.

- α: The angle between the wall and the signal path.

- w_t and w_r: The distances from the transmitter and receiver to the wall.

- w: The total wall width.

Now, using the Law of Cosines (al-Kashi's Theorem) in triangle ABC, we can express the total NLoS distance AC as:

$$AC^2 = AB^2 + BC^2 - 2 \cdot AB \cdot BC \cdot \cos(2\theta)$$

If we perform all the calculations to determine the values of AB and BC, we find that

$$AC^2 = \frac{1}{\sin^2 \alpha} \left((w - w_t)^2 + (w - w_r)^2 + 2 \cdot (w - w_t) \cdot (w - w_r) \cdot \left(1 - 2\sin^2(\alpha) \right) \right)$$

Let $AC = d$ and solve for $\sin^2(\alpha)$ by rearranging the equation. We find the value of $\sin \alpha$ is:

$$\sin \alpha = \sqrt{\frac{(w - w_t)^2 + (w - w_r)^2 + 2 \cdot (w - w_t) \cdot (w - w_r)}{d^2 + 4 \cdot (w - w_t) \cdot (w - w_r)}}$$

Finally, we substitute this value of $\sin \alpha$ into the formulas for AB and BC:

$$AB = \frac{w - w_t}{\sqrt{\frac{(w-w_t)^2 + (w-w_r)^2 + 2 \cdot (w-w_t) \cdot (w-w_r)}{d^2 + 4 \cdot (w-w_t) \cdot (w-w_r)}}}, \quad BC = \frac{w - w_r}{\sqrt{\frac{(w-w_t)^2 + (w-w_r)^2 + 2 \cdot (w-w_t) \cdot (w-w_r)}{d^2 + 4 \cdot (w-w_t) \cdot (w-w_r)}}}$$

Both AB and BC share a common denominator, which simplifies to:

$$AB = \frac{(w - w_t) \cdot \sqrt{d^2 + 4 \cdot (w - w_t) \cdot (w - w_r)}}{2w - w_t - w_r}$$

$$BC = \frac{(w - w_r) \cdot \sqrt{d^2 + 4 \cdot (w - w_t) \cdot (w - w_r)}}{2w - w_t - w_r}$$

Path-Length Difference and Phase Difference in the Wall-Reflected NLoS Scenario

To calculate the path-length difference and phase difference in the wall-reflected Non-Line-of-Sight (NLoS) scenario, we proceed by considering the path-length difference for the first wall reflection. The path-length difference is defined as:

$$\Delta d_{1\text{wall}} = x_1 + x_1' - d$$
$$\Delta d_{1\text{wall}} = \frac{w_r \cdot \sqrt{d^2 + 4 \cdot w_t \cdot w_r}}{w_t + w_r} + \frac{w_t \cdot \sqrt{d^2 + 4 \cdot w_t \cdot w_r}}{w_t + w_r} - d$$

Simplifying the expression, we get the path-length difference:

$$\Delta d_{1\text{wall}} = \sqrt{d^2 + 4 \cdot w_t \cdot w_r} - d$$

Now, for the phase difference based on the path-length difference:

$$\Delta \phi_{1\text{wall}} = \frac{2\pi \Delta d_{1\text{wall}}}{\lambda}$$

Substituting the simplified form of $\Delta d_{1\text{wall}}$:

$$\Delta \phi_{1\text{wall}} = \frac{2\pi}{\lambda} \left(\sqrt{d^2 + 4 \cdot w_t \cdot w_r} - d \right)$$

Where:

- $\Delta \phi_{1\text{wall}}$ is the phase difference,

- $\Delta d_{1\text{wall}}$ is the path-length difference,

- λ is the wavelength of the transmitted signal.

Next, we calculate the path-length difference and phase difference for the second wall reflection. We define the total path-length difference for the second wall reflection as:

$$\Delta d_{2\text{wall}} = x + x' - d$$

Where:

- x is the horizontal distance between the transmitter (Tx) and the reflection point on the wall.

- x' is the horizontal distance between the reflection point on the wall and the receiver (Rx).

- d_1 is the direct line-of-sight (LoS) distance between the transmitter and the receiver.

The phase difference $\Delta\phi_{2\text{wall}}$ is given by:

$$\Delta\phi_{2\text{wall}} = \frac{2\pi \cdot \Delta d_{2\text{wall}}}{\lambda}$$

Where:

- $\Delta\phi_{2\text{wall}}$ is the phase difference,

- $\Delta d_{2\text{wall}}$ is the path-length difference,

- λ is the wavelength of the signal.

Finally, performing the calculations for the path-length difference:

$$\Delta d_{2\text{wall}} = \frac{(w_r \cdot \sqrt{d^2 + 4 \cdot w_t \cdot w_r})}{w_t + w_r} + \frac{(w_t \cdot \sqrt{d^2 + 4 \cdot w_t \cdot w_r})}{w_t + w_r} - d$$

Where:

- w_r and w_t represent the distances from the receiver and transmitter to the wall.

- d is the direct LoS distance

Now we calculate the phase difference $\Delta\phi_{2\text{wall}}$ as:

$$\Delta\phi_{\text{total\_wall}} = \Delta\phi_{1\text{wall}} + \Delta\phi_{2\text{wall}}$$

Substituting the previously calculated expressions for $\Delta\phi_{1\text{wall}}$ and $\Delta\phi_{2\text{wall}}$:

$$\Delta\phi_{\text{total\_wall}} = \frac{2\pi}{\lambda}\left(\sqrt{d^2 + 4 \cdot w_t \cdot w_r} - d\right) + \frac{2\pi}{\lambda}\left(\frac{w_r \cdot \sqrt{d^2 + 4 \cdot w_t \cdot w_r}}{w_t + w_r} + \frac{w_t \cdot \sqrt{d^2 + 4 \cdot w_t \cdot w_r}}{w_t + w_r} - d\right)$$

The total phase difference for the wall-reflected Non-Line-of-Sight (NLoS) paths is calculated by summing the phase differences from both the first and second wall reflections. This gives us the total phase difference due to the walls:

Total Phase Difference for the 5-Ray Model

To compute the total phase difference for the 5-ray model, we are required to incorporate the phase differences from the floor and roof reflections that were calculated using the 3-ray model. So we can define that the total phase difference $\Delta\phi_{\text{total}}$ for the 5-ray model as the sum of the phase differences from the wall reflections and those from the roof and floor reflections:

$$\Delta\phi_{\text{total}} = \Delta\phi_{\text{total\_wall}} + \Delta\phi_{\text{roof}} + \Delta\phi_{\text{floor}}$$

Where:

- $\Delta\phi_{\text{roof}}$ is the phase difference due to the roof reflection (from the 3-ray model),

- $\Delta\phi_{\text{floor}}$ is the phase difference due to the floor reflection (from the 3-ray model).

Thus, the total phase difference for the 5-ray model is given by:

$$\Delta\phi_{\text{total}} = \frac{2\pi}{\lambda}\left(\sqrt{d^2 + 4\cdot w_t \cdot w_r} - d\right) + \frac{2\pi}{\lambda}\left(\frac{w_r \cdot \sqrt{d^2 + 4\cdot w_t \cdot w_r}}{w_t + w_r} + \frac{w_t \cdot \sqrt{d^2 + 4\cdot w_t \cdot w_r}}{w_t + w_r} - d_1\right) + \Delta\phi_{\text{roof}} + \Delta\phi_{\text{floor}}$$

Or

$$\Delta\phi_{\text{roof-floor}} = \frac{2\pi}{\lambda}\left(\frac{\sqrt{d^2 - 4\cdot(H - h_t)\cdot(H - h_r)}\cdot((H - h_t) + (H - h_r))}{\sqrt{(H - h_t)^2 + (H - h_r)^2 - 2\cdot(H - h_t)\cdot(H - h_r)}}\right)$$

So we define the total phase difference for the 5-ray model as :

$$\begin{aligned}
\Delta\phi_{\text{total}} &= \frac{2\pi}{\lambda}\left(\sqrt{d^2 + 4\cdot w_t \cdot w_r} - d\right) \\
&+ \frac{2\pi}{\lambda}\left(\frac{w_r \cdot \sqrt{d^2 + 4\cdot w_t \cdot w_r}}{w_t + w_r} + \frac{w_t \cdot \sqrt{d^2 + 4\cdot w_t \cdot w_r}}{w_t + w_r} - \sqrt{(h_t - h_r)^2 + d^2}\right) \\
&+ \frac{2\pi}{\lambda}\left(\frac{\sqrt{d^2 - 4\cdot(H - h_t)\cdot(H - h_r)}\cdot((H - h_t) + (H - h_r))}{\sqrt{(H - h_t)^2 + (H - h_r)^2 - 2\cdot(H - h_t)\cdot(H - h_r)}}\right)
\end{aligned}$$

We calculated the total phase difference for the 5-ray model by adding the contributions from both wall reflections, as well as the roof and floor reflections from the 3-ray model. Each time we add more rays to the model, we apply the 3-ray model to handle the primary reflections (floor, roof, and direct path), and then we add the additional rays.

3.2.4 Received Power

The received power P_r is a fundamental parameter in wireless communication that represents the strength of the signal arriving at the receiver after undergoing various propagation phenomena such as reflection, diffraction, and attenuation. It is mathematically defined as the squared magnitude of the total received signal $r_{\text{tot}}(t)$, averaged over time:

$$P_r = \left\langle |r_{\text{tot}}(t)|^2 \right\rangle$$

Where:

- $r_{\text{tot}}(t)$: the total received signal.

- $\langle \cdot \rangle$: The time-averaging operation .

The total received signal $r_{\text{tot}}(t)$ is the sum of all individual signal components arriving at the receiver from different paths:

$$r_{\text{tot}}(t) = \sum_{i=1}^{N} r_i(t)$$

Where:

- N is the number of signal components (e.g., the direct path, ground-reflected path, wall-reflected paths, etc.).

- $r_i(t)$ is the received signal from the i-th path.

3-Ray Propagation Model

In the 3-ray propagation model, the total received signal is the sum of three components:

$$r_{\text{los}}(t) = \frac{\lambda}{4\pi d}\sqrt{G}e^{-j\frac{2\pi d}{\lambda}}e^{j\omega t}$$

$$r_{\text{nlos1}}(t) = \frac{\lambda}{4\pi(x+x')}\sqrt{G}e^{-j\frac{2\pi(x+x')}{\lambda}}e^{j\omega t}$$

$$r_{\text{nlos2}}(t) = \frac{\lambda}{4\pi(x_1+x_1')}\sqrt{G}e^{-j\frac{2\pi(x_1+x_1')}{\lambda}}e^{j\omega t}$$

$$r_{\text{tot}}(t) = \frac{\lambda}{4\pi}\sqrt{G}e^{j\omega t}\left(\frac{e^{-j\frac{2\pi d}{\lambda}}}{d} + \frac{e^{-j\frac{2\pi(x+x')}{\lambda}}}{x+x'} + \frac{e^{-j\frac{2\pi(x_1+x_1')}{\lambda}}}{x_1+x_1'}\right)$$

Where:

- λ is the wavelength.

- d is the direct LoS distance between the transmitter and receiver.

- G is the gain of the antennas.

- ω is the angular frequency.

- x and x' are the horizontal distances for the ground-reflected path.

- x_1 and x_1' are the horizontal distances for the roof-reflected path.

56

We define the path-length differences Δd_1 and Δd_2 for both NLoS paths as follows:

$$\Delta d_1 = d - (x + x'), \quad \Delta d_2 = d - (x_1 + x_1')$$

The phase differences are then given by:

$$\Delta \phi_1 = \frac{2\pi}{\lambda} \Delta d_1, \quad \Delta \phi_2 = \frac{2\pi}{\lambda} \Delta d_2$$

Thus, the total received signal r_{tot} can be written as:

$$r_{\text{tot}} = \frac{4\pi}{\lambda} \sqrt{G} e^{j\omega t} \cdot e^{-j \frac{2\pi d}{\lambda}} \cdot \left[1 + \frac{d}{x_1 + x_1'} e^{-j\Delta\phi_1} + \frac{d}{x + x'} e^{-j\Delta\phi_2} \right] \tag{3.12}$$

We define z as:

$$z = \frac{d}{x_1 + x_1'} e^{-j\Delta\phi_1} + \frac{d}{x + x'} e^{-j\Delta\phi_2}$$

Using Euler's formula $e^{-j\theta} = \cos(\theta) - j\sin(\theta)$, we rewrite z as:

$$z = \frac{d}{x_1 + x_1'} \left(\cos(\Delta\phi_1) - j\sin(\Delta\phi_1) \right) + \frac{d}{x + x'} \left(\cos(\Delta\phi_2) - j\sin(\Delta\phi_2) \right)$$

Now, separate z into its real and imaginary parts:

$$z = \left(\frac{d}{x_1 + x_1'} \cos(\Delta\phi_1) + \frac{d}{x + x'} \cos(\Delta\phi_2) \right) - j \left(\frac{d}{x_1 + x_1'} \sin(\Delta\phi_1) + \frac{d}{x + x'} \sin(\Delta\phi_2) \right)$$

Define the real part a and imaginary part b of z:

$$a = \frac{d}{x_1 + x_1'} \cos(\Delta\phi_1) + \frac{d}{x + x'} \cos(\Delta\phi_2)$$

$$b = \frac{d}{x_1 + x_1'} \sin(\Delta\phi_1) + \frac{d}{x + x'} \sin(\Delta\phi_2)$$

Thus, z can be written as:

$$z = a - jb$$

Now, calculate $|1 + z|^2$:

$$|1 + z|^2 = (1 + a)^2 + b^2$$

Substituting a and b:

$$|1+z|^2 = \left(1 + \frac{d}{x_1 + x_1'} \cos(\Delta\phi_1) + \frac{d}{x + x'} \cos(\Delta\phi_2) \right)^2 + \left(\frac{d}{x_1 + x_1'} \sin(\Delta\phi_1) + \frac{d}{x + x'} \sin(\Delta\phi_2) \right)^2$$

We suppose that :

$$r_1 = \frac{d}{x_1 + x_1'}$$

$$r_2 = \frac{d}{x + x'}$$

We try to Expand both terms of $|1 + z|^2$ term to get the final total received signal equation.

$$|1 + z|^2 = (1 + r_1 \cos(\Delta\phi_1) + r_2 \cos(\Delta\phi_2))^2 + (r_1 \sin(\Delta\phi_1) + r_2 \sin(\Delta\phi_2))^2$$

$$|1+z|^2 = 1 + r_1^2 \cos^2(\Delta\phi_1) + r_2^2 \cos^2(\Delta\phi_2) + 2r_1 \cos(\Delta\phi_1) + 2r_2 \cos(\Delta\phi_2) + 2r_1 r_2 \cos(\Delta\phi_1) \cos(\Delta\phi_2)$$

$$+ r_1^2 \sin^2(\Delta\phi_1) + r_2^2 \sin^2(\Delta\phi_2) + 2r_1 r_2 \sin(\Delta\phi_1) \sin(\Delta\phi_2)$$

Since $\cos^2(\Delta\phi) + \sin^2(\Delta\phi) = 1$, we can group terms for r_1 and r_2:

$$|1 + z|^2 = 1 + r_1^2(\cos^2(\Delta\phi_1) + \sin^2(\Delta\phi_1)) + r_2^2(\cos^2(\Delta\phi_2) + \sin^2(\Delta\phi_2))$$

$$+ 2r_1 \cos(\Delta\phi_1) + 2r_2 \cos(\Delta\phi_2) + 2r_1 r_2 (\cos(\Delta\phi_1) \cos(\Delta\phi_2) + \sin(\Delta\phi_1) \sin(\Delta\phi_2))$$

Using $\cos^2(\Delta\phi) + \sin^2(\Delta\phi) = 1$, this simplifies to:

$$|1 + z|^2 = 1 + r_1^2 + r_2^2 + 2r_1 \cos(\Delta\phi_1) + 2r_2 \cos(\Delta\phi_2) + 2r_1 r_2 \cos(\Delta\phi_1 - \Delta\phi_2)$$

So the final expression of $r_t ot$

$$r_{\text{tot}}(t) = \frac{\lambda}{4\pi} \sqrt{G} e^{j\omega t} \left(\frac{e^{-j\frac{2\pi d}{\lambda}}}{d} + \frac{e^{-j\frac{2\pi(x+x')}{\lambda}}}{x + x'} + \frac{e^{-j\frac{2\pi(x_1+x_1')}{\lambda}}}{x_1 + x_1'} \right)$$

$$r_{\text{tot}}(t) = \frac{\lambda}{4\pi} \sqrt{G} e^{j\omega t} \left(\frac{1}{d} \cos\left(\frac{2\pi d}{\lambda} \right) + \frac{1}{x + x'} \cos\left(\frac{2\pi(x + x')}{\lambda} \right) + \frac{1}{x_1 + x_1'} \cos\left(\frac{2\pi(x_1 + x_1')}{\lambda} \right) \right)$$

Now, We define the total received power in the 3-ray model as follows:

$$P_r = \left\langle |r_{\text{los}}(t) + r_{\text{nlos1}}(t) + r_{\text{nlos2}}(t)|^2 \right\rangle$$

$$P_r = \frac{\lambda^2 G}{(4\pi d)^2} \cdot \left(1 + r_1^2 + r_2^2 + 2r_1 \cos(\Delta\phi_1) + 2r_2 \cos(\Delta\phi_2) + 2r_1 r_2 \cos(\Delta\phi_1 - \Delta\phi_2) \right)$$

We define $\gamma(\Delta\phi_1, \Delta\phi_2)$ as:

$$\gamma(\Delta\phi_1, \Delta\phi_2) = \left(1 + r_1^2 + r_2^2 + 2r_1 \cos(\Delta\phi_1) + 2r_2 \cos(\Delta\phi_2) + 2r_1 r_2 \cos(\Delta\phi_1 - \Delta\phi_2) \right)$$

where:

$$r_1 = \frac{d}{x_1 + x_1'}$$

$$r_2 = \frac{d}{x + x'}$$

$$P_r = \frac{\lambda^2 G}{(4\pi d)^2} \left(1 + \frac{d^2}{(x_1 + x_1')^2} + \frac{d^2}{(x + x')^2} + 2\frac{d}{x_1 + x_1'} \cos(\Delta\phi_1) + 2\frac{d}{x + x'} \cos(\Delta\phi_2) + 2\frac{d^2}{(x_1 + x_1')(x + x')} \cos(\Delta\phi_1 - \Delta \right.$$

Then, the total received power P_{total} can be expressed as:

$$P_{\text{total}} = P_{\text{los}} \left(1 + \gamma(\Delta\phi_1, \Delta\phi_2) \right)$$

5-Ray Propagation Model

In the 5-ray model, two additional components are considered, representing the reflections from two side-walls. The total received signal in this case is:

$$r_{\text{los}}(t) = \frac{\lambda}{4\pi d} \sqrt{G} e^{-j\frac{2\pi d}{\lambda}} e^{j\omega t}$$

$$r_{\text{nlos\_ground}}(t) = \frac{\lambda}{4\pi(x + x')} \sqrt{G} e^{-j\frac{2\pi(x+x')}{\lambda}} e^{j\omega t}$$

$$r_{\text{nlos\_roof}}(t) = \frac{\lambda}{4\pi(x_1 + x_1')} \sqrt{G} e^{-j\frac{2\pi(x_1+x_1')}{\lambda}} e^{j\omega t}$$

$$r_{\text{nlos\_wall1}}(t) = \frac{\lambda}{4\pi(w_1 + w_1')} \sqrt{G} e^{-j\frac{2\pi(w_1+w_1')}{\lambda}} e^{j\omega t}$$

$$r_{\text{nlos\_wall2}}(t) = \frac{\lambda}{4\pi(w_2 + w_2')} \sqrt{G} e^{-j\frac{2\pi(w_2+w_2')}{\lambda}} e^{j\omega t}$$

So the Total Received Signal is given as :

$$r_{\text{tot}}(t) = r_{\text{los}}(t) + r_{\text{nlos1}}(t) + r_{\text{nlos2}}(t) + r_{\text{nloswall1}}(t) + r_{\text{nloswall2}}(t)$$

$$r_{\text{tot}}(t) = \frac{\lambda}{4\pi} \sqrt{G} e^{j\omega t} \left(\frac{e^{-j\frac{2\pi d}{\lambda}}}{d} + \frac{e^{-j\frac{2\pi(x+x')}{\lambda}}}{x + x'} + \frac{e^{-j\frac{2\pi(x_1+x_1')}{\lambda}}}{x_1 + x_1'} + \frac{e^{-j\frac{2\pi(w_1+w_1')}{\lambda}}}{w_1 + w_1'} + \frac{e^{-j\frac{2\pi(w_2+w_2')}{\lambda}}}{w_2 + w_2'} \right)$$

Where:

- λ: Wavelength of the signal.

- d: Direct LoS distance between the transmitter and receiver.

- G: Gain of the antennas.

- ω: Angular frequency of the signal.

- x and x': Horizontal distances for the ground-reflected path.

- x_1 and x_1': Horizontal distances for the roof-reflected path.

- w_1 and w_1': Horizontal distances for the first wall-reflected path.

- w_2 and w_2': Horizontal distances for the second wall-reflected path.

Thus, the received power in the 5-ray model becomes:

$$P_r = \left\langle |r_{\text{los}}(t) + r_{\text{nlos1}}(t) + r_{\text{nlos2}}(t) + r_{\text{nloswall1}}(t) + r_{\text{nloswall2}}(t)|^2 \right\rangle$$

$$P_r = \frac{\lambda^2 G}{(4\pi)^2} \left\langle \left| \frac{e^{-j\frac{2\pi d}{\lambda}}}{d} + \frac{e^{-j\frac{2\pi(x+x')}{\lambda}}}{x+x'} + \frac{e^{-j\frac{2\pi(x_1+x_1')}{\lambda}}}{x_1+x_1'} + \frac{e^{-j\frac{2\pi(w_1+w_1')}{\lambda}}}{w_1+w_1'} + \frac{e^{-j\frac{2\pi(w_2+w_2')}{\lambda}}}{w_2+w_2'} \right|^2 \right\rangle$$

$$P_r = P_{\text{los}} \left| 1 + r_{\text{ground}} e^{-j\Delta\phi_{\text{ground}}} + r_{\text{roof}} e^{-j\Delta\phi_{\text{roof}}} + r_{\text{wall1}} e^{-j\Delta\phi_{\text{wall1}}} + r_{\text{wall2}} e^{-j\Delta\phi_{\text{wall2}}} \right|^2$$

Where:

- $P_{\text{los}} = \frac{\lambda^2 G}{(4\pi d)^2}$ is the power for the direct path.

- $r_{\text{ground}} = \frac{d}{x+x'}$, $r_{\text{roof}} = \frac{d}{x_1+x_1'}$, $r_{\text{wall1}} = \frac{d}{w_1+w_1'}$, and $r_{\text{wall2}} = \frac{d}{w_2+w_2'}$ are the ratios of the LoS path distance d to the respective path distances.

- $\Delta\phi_{\text{ground}}, \Delta\phi_{\text{roof}}, \Delta\phi_{\text{wall1}}$, and $\Delta\phi_{\text{wall2}}$ are the phase shifts introduced by the ground, roof, and wall reflections.

After performing detailed calculations, we arrive at the final expression for the total received power in the 5-ray model. Due to the complexity introduced by multiple reflection paths—specifically from the ground, roof, and two walls—the process involves summing contributions from each path while accounting for the amplitude and phase shifts. The 5-ray model requires careful handling of these factors to accurately reflect the combined impact of the direct and reflected signals, leading to a more comprehensive but intricate expression for the received power.

$$r_{\text{tot}} = \left(\frac{\lambda}{4\pi d}\right)^2 G \left[1 + \sum_{k=1}^{4} \frac{d^2}{(x_k+x_k')^2} + 2\sum_{k=1}^{4} \frac{d}{x_k+x_k'} \cos(\Delta\phi_k) + 2\sum_{i<j} \left(\frac{d}{x_i+x_i'}\right) \left(\frac{d}{x_j+x_j'}\right) \cos(\Delta\phi_i - \Delta\phi_j) \right]$$

From the expression for r_{tot} in the 5-ray model, we can generalize this model to define a general equation for an n-ray model by extending the summation limits to n. This yields the following equation for $r_{\text{tot}}^{(n\text{-ray})}$:

$$r_{\text{tot}}^{(n\text{-ray})} = \left(\frac{\lambda}{4\pi d}\right)^2 G \left[1 + \sum_{k=1}^{n} \frac{d^2}{(x_k+x_k')^2} + 2\sum_{k=1}^{n} \frac{d}{x_k+x_k'} \cos(\Delta\phi_k) + 2\sum_{i<j} \left(\frac{d}{x_i+x_i'}\right) \left(\frac{d}{x_j+x_j'}\right) \cos(\Delta\phi_i - \Delta\phi_j) \right]$$

This generalized equation $r_{\text{tot}}^{(n\text{-ray})}$ allows for modeling the total received signal with an arbitrary number n of reflected rays, considering both amplitude and phase effects for each reflection path.

3.2.5 Results of the Localization Algorithm B

To validate the effectiveness of the multi-ray model (the 3-ray and 5-ray models) in accurately locating an RFID-tagged object within a room, a series of simulations were conducted using Python. The primary objective of these simulations was to determine if the proposed ray model approach could reliably estimate the object's position based on known phases of signal propagation.

Simulation Steps

1.Initialization and Object Point Definition The simulations began by defining a known position for the tagged object, necessary for calculating the phase value of the signal reaching this location. This calculated phase is termed the "measured phase." For this particular simulation, the object was assumed to be located at coordinates (4.5, 2.5, 0), with the z-coordinate being zero, indicating that the object was placed on the floor. Multiple tests were conducted, and this is one example using these known coordinates.

2.Defining Possible Tag Positions (X and Y Ranges) :

To explore potential object positions, the simulation defined ranges across both X and Y coordinates, creating a grid of possible tag locations throughout the room. This enabled phase predictions for each potential tag position, which were then compared with the measured phase for accuracy. In the conducted simulation, the localization process involved two main steps, including parallel and orthogonal movement relative to the tagged object's location. This approach aligns with the methodologies in the referenced article, providing a structured method for achieving precise positioning.

- Parallel Movement to Determine X

The process started with parallel movement to determine the X-coordinate of the tagged object as shown in image 3.19. Here, the simulation calculated predicted phases for various X positions and selected the one with the highest correlation to the measured phase. This position, where the predicted phase response was maximized, provided a reliable estimate of the tagged object's X location.

- Fixing X and Performing Orthogonal Movement to Determine Y After estimating the X-coordinate, the simulation fixed this value and proceeded with orthogonal movements along the Y-axis as shown in image 3.20. While keeping X constant, the simulation generated a series of positions in the form (4.4898, Y, 0), with Y values ranging from 0 to 10 meters in set intervals. This thorough grid search enabled an accurate comparison between measured and predicted phases. The Y-coordinate that produced the closest phase match to the measured phase was then selected, completing the localization of the object within the room.
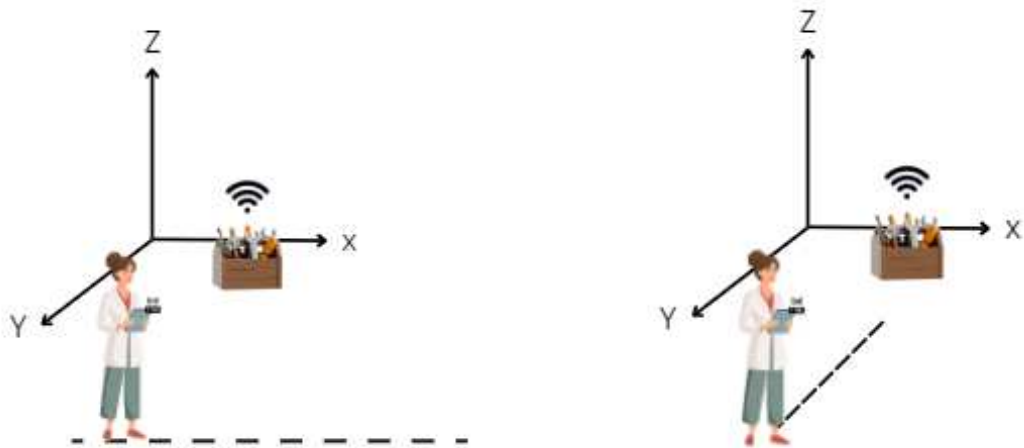
Figure 3.19: User Movements for Object Localization: Parallel and Orthogonal Phases

3.Phase Prediction and Comparison

For each potential tag position, the simulation computed predicted phases using the multi-ray model and compared them with the measured phases along discrete robot positions on the X-axis. The simulation iterated over possible positions and calculated the Mean Squared Error (MSE) between measured and predicted phases, allowing the identification of the tag position that most closely matched the actual object position.

In the following figure 3.20the measured phase as the robot moves along the X-axis. The peak phase position is of particular importance, as it indicates the location along the X-axis that corresponds most closely to the tag's actual X-coordinate. By identifying this peak, the algorithm can effectively estimate the X-coordinate of the tag.
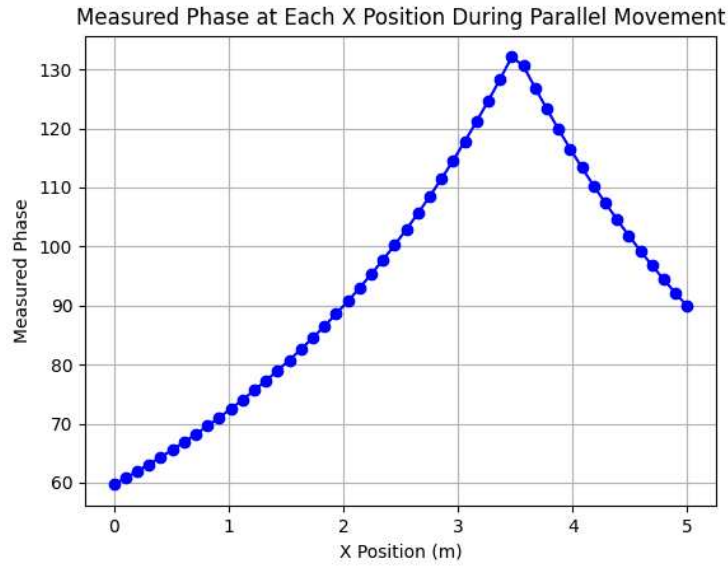
Figure 3.20: Measured Phase at Each X Position During Parallel Movement

4.Estimation Results

The simulation's output yielded an estimated X-coordinate of approximately 4.4898, aligning closely with the actual object's X-coordinate of 4.5. Additionally, potential tag positions along the Y-axis were explored, leading to an estimated Y-coordinate of 0.0, consistent with the object's actual Y position. These results confirm the model's accuracy in locating the tagged object, effectively validating the multi-ray model's capability in handling complex multipath environments.

The image 3.21 shows the accuracy of the localization process, specifically focusing on how closely the estimated coordinates align with the actual position of the tag along both the X and Y axes. After determining the X-coordinate during the parallel movement phase, the orthogonal movement allowed for precise localization along the Y-axis. This accurate positioning confirms the effectiveness of the proposed localization algorithm, demonstrating its reliability in pinpointing the tag's location in a controlled environment.
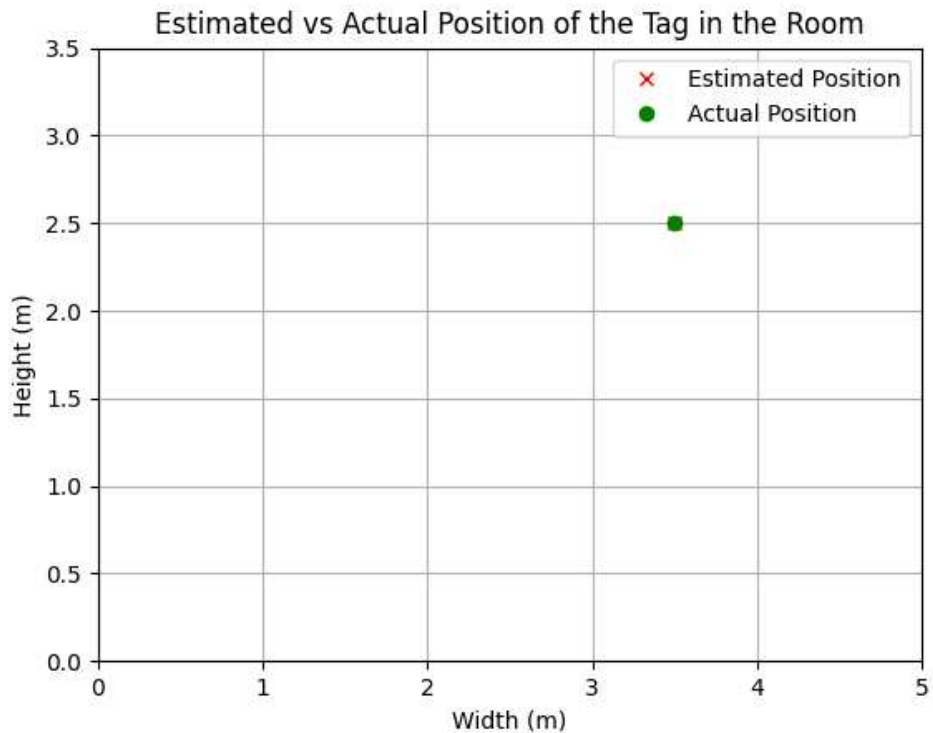
Figure 3.21: Comparison of Estimated and Actual Tag Position with Phase Prediction Analysis During Parallel Movement

The next breakdown shown in figure 3.22 presents the comparison between measured and predicted phase values during the two key stages of the localization process: parallel and orthogonal movements. This examination evaluates the accuracy of the estimated coordinates for the tagged object's location.

1. Measured vs Predicted Phases for the Parallel Movement :

- The figure displays the relationship between the measured and predicted phase values as the user moves along the X-axis, maintaining a parallel trajectory relative to the tagged object's estimated position. The close alignment between the measured (blue) and predicted (red) phases indicates that the estimated X-coordinate (4.4898) is highly accurate, validating the initial parallel movement phase of the localization process.

2.Measured vs Predicted Phases for the Orthogonal Movement :

- The figure depicts the measured and predicted phases as the user moves along the Y-axis (after finding and fixing the X-coordinate). As shown, the measured phase (blue) and predicted phase (red) curves align closely, with the best estimated Y-coordinate at approximately 5.9184. The small differences between the two sets of phase values confirm the effectiveness of the orthogonal movement phase in refining the localization of the tagged object within the room.
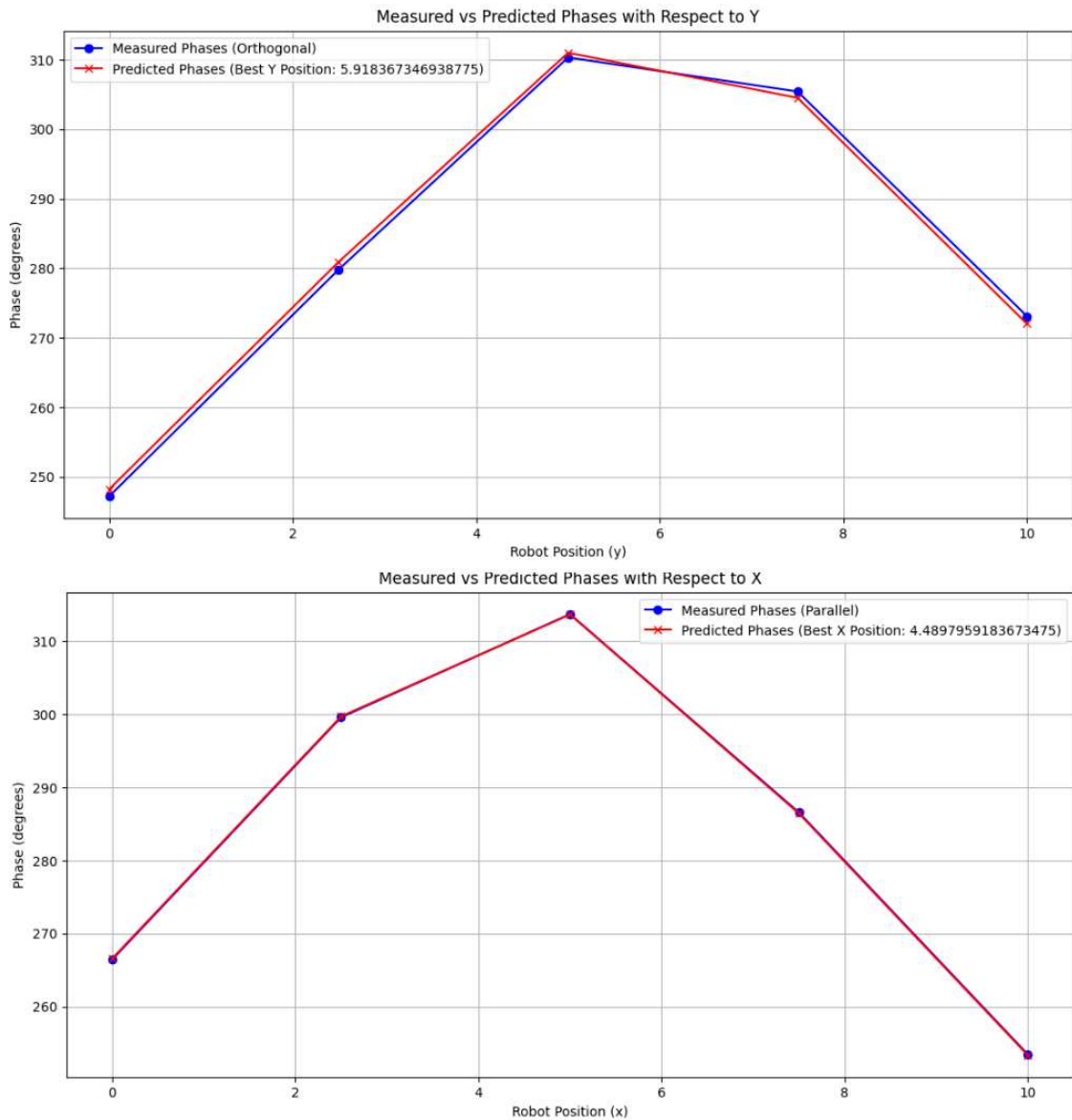
Figure 3.22: Measured vs Predicted Phases During Parallel and Orthogonal Movements for Localization

3.3 Comparative Analysis of Algorithm A and Algorithm B

To gain a clearer understanding of the capabilities and limitations of each localization approach, it is important to conduct a comparative analysis of both algorithms A and B. This helps to better evaluate how well each one addresses specific challenges in various environments. Algorithm A, which leverages a simple RSSI-based grid search, is well-suited for smaller, less complex spaces. In contrast, Algorithm B contains a sophisticated multi-ray reflection model, making it more effective in environments where multipath inter-

ference significantly impacts signal propagation. Through this comparison, we can identify the strengths and weaknesses of each algorithm, determining which is more suitable for our case. **- Algorithm A**: Focused on a grid-based localization strategy with RSSI metrics to locate objects. This solution is suited for small and controlled environments where signal reflections and multipath effects are limited.

- Algorithm B: Developed using the Three-Ray Ground Reflection Model (and 5-Ray Reflection model) , this algorithm addresses the complexity of larger environments with multiple reflective surfaces introduced specialy with metals objects .

3.3.1 Strengths and Limitations

While Algorithm A is suitable for straightforward scenarios, Algorithm B provides a robust solution for more complex, multipath-rich environments. If extended to the n-ray model, Algorithm B could potentially provide even greater accuracy by considering additional reflections. The following table 3.1 highlight the strengths and limitations points for each solution .

Algorithm	Strengths	Limitations
A	- Fast and straightforward, suitable for quick localization in smaller or open environments. - Effective where environmental factors, like reflections and obstacles, are minimal.	- Limited effectiveness in large or complex environments where multipath interference affects accuracy. - Reliance on RSSI measurements alone, which can be affected by attenuation and obstacles.
B	- Provides high accuracy in complex environments due to handling multipath interference. - Utilizes a multi-ray reflection model, accounting for various reflection paths for enhanced precision.	- Computationally intensive, needing significant processing power for multiple signal path calculations. - Requires detailed environmental modeling, including geometry and reflective surfaces.

Table 3.1: Comparative Analysis of Algorithm A and Algorithm B

4
Conclusions

In this thesis, we investigated the challenge of localizing metallic lost tools using UHF RFID systems in industrial environments, focusing on the complexities introduced by metallic surfaces. By developing two distinct algorithms, A and B, we explored different approaches to enhancing the accuracy and reliability of RFID-based localization.

If we try to summarise the main ideas, algorithm A, which relies on a grid-based movement and RSSI measurements, proved effective in smaller environments with minimal interference. It demonstrated a straightforward implementation and quick responsiveness, making it suitable for settings where signal reflection and multipath effects are less. Regardless, as the environment's complexity increased, Algorithm A faced limitations in terms of accuracy, especially in settings with extensive metallic interference.

To address these limitations, Algorithm B was developed using a more advanced approach, incorporating the Three-Ray Ground Reflection Model, and subsequently extending it to a Five-Ray Model to include wall reflections. This model allowed for a more detailed analysis of signal paths and provided greater resilience to multipath interference by taking into account reflections from multiple surfaces. Algorithm B's detailed trigonometric and phase-difference calculations offered enhanced accuracy in complex environments, such as warehouses and industrial spaces with metallic surfaces. Furthermore, by building upon the 5-ray model, we extend our work to create an N-ray reflection model. This model accommodates scenarios involving a direct signal and $(n-1)$ indirect signals, providing a more comprehensive approach to multipath signal analysis. To the best of our knowledge, this analytical approach has not been previously documented in the literature. Future work in this area will involve introducing and discussing this new development to showcase its potential applications and benefits in signal localization.

Finally, the findings from this study demonstrate the feasibility of using advanced RFID models for reliable localization in environments that typically hinder signal propagation. By mitigating issues such as signal attenuation and interference, Algorithm B shows potential for integration into existing industrial systems, where it could significantly improve operational efficiency by rapidly locating misplaced metallic objects.

References

[1] P. V. Nikitin, K. Rao, and S. Lazar, "An overview of near field uhf rfid," in *2007 IEEE international conference on RFID*, IEEE, 2007, pp. 167–174.

[2] Y. Duroc and S. Tedjini, "Rfid: A key technology for humanity," *Comptes Rendus. Physique*, vol. 19, no. 1-2, pp. 64–71, 2018.

[3] R. Weinstein, "Rfid: A technical overview and its application to the enterprise," *IT professional*, vol. 7, no. 3, pp. 27–33, 2005.

[4] V. Chawla and D. S. Ha, "An overview of passive rfid," *IEEE Communications Magazine*, vol. 45, no. 9, pp. 11–17, 2007.

[5] F. Chiariotti and L. Badia, "Strategic age of information aware interaction over a relay channel," *IEEE Transactions on Communications*, 2023.

[6] J. Doe, *Rfid middleware: Functions and benefits*, Accessed: 2023-07-19, 2023.

[7] C. Floerkemeier and M. Lampe, "Rfid middleware design: Addressing application requirements and rfid constraints," in *Proceedings of the 2005 joint conference on Smart objects and ambient intelligence: innovative context-aware services: usages and technologies*, 2005, pp. 219–224.

[8] A. Buratto, H. Tuwei, and L. Badia, "Optimizing sensor data transmission in collaborative multi-sensor environments," in *2023 IEEE International Conference on Communication, Networks and Satellite (COMNETSAT)*, IEEE, 2023, pp. 635–639.

[9] A. Zancanaro, G. Cisotto, and L. Badia, "Tackling age of information in access policies for sensing ecosystems," *Sensors*, vol. 23, no. 7, p. 3456, 2023.

[10] U. Singh and A. Sharad, "The smart city: A holistic approach," in *2020 11th International Conference on Computing, Communication and Networking Technologies (ICCCNT)*, IEEE, 2020, pp. 1–7.

[11] W.-T. Sung and C.-Y. Lu, "Smart warehouse management based on iot architecture," in *2018 International Symposium on Computer, Consumer and Control (IS3C)*, 2018, pp. 169–172.

[12] T. Deyle, M. S. Reynolds, and C. C. Kemp, "Finding and navigating to household objects with uhf rfid tags by optimizing rf signal strength," in *2014 IEEE/RSJ International Conference on Intelligent Robots and Systems*, IEEE, 2014, pp. 2579–2586.

[13] M. N. Borenovic and A. M. Neskovic, "Comparative analysis of rssi, snr and noise level parameters applicability for wlan positioning purposes," in *IEEE EUROCON 2009*, IEEE, 2009, pp. 1895–1900.

[14] A. Rech, M. Pagin, L. Badia, *et al.*, "Clustering-based downlink scheduling of irs-assisted communications with reconfiguration constraints," *IEEE Transactions on Wireless Communications*, 2024.

[15] E. Pereira, S. Júnior, L. F. V. Silva, *et al.*, "Rfid tags for on-metal applications: A brief survey," *Technologies*, vol. 12, no. 5, p. 58, 2024.

[16] L. Badia, V. Mancuso, and M. A. Marsan, "Adversarial obstruction of millimeter wave links," in *2023 21st Mediterranean Communication and Computer Networking Conference (MedComNet)*, IEEE, 2023, pp. 101–110.

[17] D. Girbau, J. Lorenzo, A. Lazaro, and R. Villarino, "Effects of antenna detuning and gain penalty on the read range of uhf rfid," in *European Workshop on Smart Objects: Systems, Technologies and Applications*, VDE, 2010, pp. 1–7.

[18] E. DiGiampaolo and F. Martinelli, "A robotic system for localization of passive uhf-rfid tagged objects on shelves," *IEEE Sensors Journal*, vol. 18, no. 20, pp. 8558–8568, 2018.

[19] J. Zhu and Z. Li, "Analysis of magnetic shielding effect on an rfid coil antenna in metallic environments with a ferrite toroid," *IEEE Transactions on Electromagnetic Compatibility*, vol. 62, no. 6, pp. 2613–2620, 2020.

[20] A. P. Sohrab, Y. Huang, M. Hussein, M. Kod, and P. Carter, "A uhf rfid tag with improved performance on liquid bottles," *IEEE Antennas and Wireless Propagation Letters*, vol. 15, pp. 1673–1676, 2016.

[21] D. Hotte, R. Siragusa, S. Tedjini, and Y. Duroc, "A new concept of uhf rfid tag for metallic object tracking with embedded cavity," in *2014 IEEE RFID Technology and Applications Conference (RFID-TA)*, IEEE, 2014, pp. 237–240.

[22] F. Fitzek, L. Badia, M. Zorzi, G. Schulte, P. Seeling, and T. Henderson, "Mobility and stability evaluation in wireless multi-hop networks using multi-player games," in *Proceedings of the 2nd workshop on Network and system support for games*, 2003, pp. 77–87.

[23] K. Çoçoli and L. Badia, "A comparative analysis of sensor fusion algorithms for miniature imu measurements," in *2023 International Seminar on Intelligent Technology and Its Applications (ISITIA)*, IEEE, 2023, pp. 239–244.

[24] F. Guidolin, M. Nekovee, L. Badia, and M. Zorzi, "A study on the coexistence of fixed satellite service and cellular networks in a mmwave scenario," in *2015 IEEE International Conference on Communications (ICC)*, IEEE, 2015, pp. 2444–2449.

[25] O. Kundacina, M. Petkovic, A. Munari, D. Vukobratovic, and L. Badia, "Move away from me! user repulsion under proximity-induced interference in owc systems," in *European Wireless 2023; 28th European Wireless Conference*, VDE, 2023, pp. 308–313.

Acknowledgments

I would like to express my sincere gratitude to everyone who has supported me throughout this journey. A deep thanks to my supervisors, for their invaluable advice, and encouragement in the successful completion of this thesis. Also, i want to thank my friends, whose constant support and constructive discussions helped me overcome numerous challenges.